The Leeuwin Current off Western Australia, 1986–1987

ROBERT L. SMITH* AND ADRIANA HUYER

College of Oceanography, Oregon State University, Corvallis, Oregon

J. STUART GODFREY AND JOHN A. CHURCH

CSIRO Division of Oceanography, Hobart, Tasmania

(Manuscript received 9 April 1990, in final form 30 August 1990)

ABSTRACT

The Leeuwin Current in the Indian Ocean off Western Australia differs from the other major eastern boundary currents, e.g., California Current, since it flows rapidly poleward against the prevailing equatorward wind. The first large-scale study of the Leeuwin Current was conducted between North West Cape (22°S) and the southwestern corner of Australia (35°S) from September 1986 to August 1987. As part of this Leeuwin Current Interdisciplinary Experiment (LUCIE), current meters were deployed along the shelf-edge (from 22° to 35°S) and across the shelf and upper slope (at 29.5° and 34°S), and CTD surveys were made out from the shelf at several latitudes. Except for about one month (January) the flow between the surface and about 250 m was strongly poleward within 100 km of the shelf-edge, with a poleward transport of about 5 Sv (Sv $\equiv 10^6$ m^3 s^{-1}). The 325-day mean currents at the shelf-edge were poleward at about 10 cm s^{-1}, opposing a mean equatorward wind stress of 0.3 dyn cm^{-2}. The monthly mean current over the upper slope exceeded 50 cm s^{-1} poleward at times and had a 325-day mean of 30 cm s^{-1}; an equatorward undercurrent existed below about 300 m and had a 325-day mean of 10 cm s^{-1} at 450 m. The strong, narrow Leeuwin Current depends on the large-scale alongshore gradient of geopotential anomaly at the sea surface, with a value greater than 2×10^{-6} m s^{-2}, which is anomalously large compared to other eastern boundary regions. The onshore geostrophic transport exceeded the offshore Ekman transport induced by the equatorward wind stress, and was presumably balanced over the upper slope and outer shelf by the offshore Ekman transport near the bottom under the Leeuwin Current. The seasonal variation in the strength of the Leeuwin Current seemed to be the result of variations in the wind stress and not in the alongshore pressure gradient, which had little seasonal dependence.

1. Introduction

The southeast Indian Ocean off Western Australia is geographically the analogue of the eastern boundary current regions in the Atlantic and Pacific oceans (Benguela, Canary, Peru, and California currents). As in these regions, the winds off Western Australia are predominantly equatorward (KNMI 1949), and one might expect to find broad equatorward flow and upwelling along the coast. However, the ocean off Western Australia behaves quite unlike the other eastern boundary regions: There is no regular, continuous equatorward flow within 1000 km of the coast (Andrews 1977) and no evidence of coastal upwelling (Wooster and Reid, 1963). Instead, the evidence from fauna (Saville-Kent 1897), ships drift (KNMI 1949) and water properties (Rochford 1969) indicate poleward flow, against the prevailing wind, along the western coast of Australia from North West Cape (22°S) to Cape Leeuwin (34.5°S). Cresswell and Golding (1980), using satellite-tracked drifters, showed that the poleward flow of warm water was fast (often >0.5 m s^{-1}), associated with predominantly cyclonic mesoscale features (eddies) on the seaward side, and continued eastward around Cape Leeuwin into the Great Australian Bight. They named the poleward surface flow the Leeuwin Current after a Dutch ship that explored eastward into the bight in the early 17th century.

Church et al. (1989) have reviewed historical and recent observations and ideas about the Leeuwin Current. A review of the theoretical models, and relevant observations, is given in Batteen and Rutherford (1990). The explanation for the anomalous behavior in this eastern boundary region seems to lie in the strength of the poleward pressure gradient in the eastern Indian Ocean: Thompson (1984) and Godfrey and Ridgway (1985) pointed out that the slope of the geopotential anomaly along the Western Australian coast is very large and could overcome the alongshore equa-

* Authors are listed in reverse alphabetical order, as appropriate for the Leeuwin Current.

Corresponding author address: Dr. Robert L. Smith, College of Oceanography, Oregon State University, Corvallis, OR 97331-5503

torward wind stress. Thompson (1987) argued that near the boundary the eastward geostrophic flow resulting from the alongshore pressure gradient is sufficient to suppress any coastal upwelling; the eastward flow downwells, deepening the surface mixed layer on the shelf and the upper slope. The alongshore pressure gradient is then balanced by the alongshore wind stress and the bottom friction acting on poleward flow over the outer shelf and upper slope.

Between September 1986 and August 1987 the Leeuwin Current Interdisciplinary Experiment (LUCIE) was conducted along the coast of Western Australia between North West Cape at 22°S and Albany at 35°S (Fig. 1). As part of this experiment, current meter moorings were deployed across and along the continental shelf-edge in order to determine the structure and variability of the Leeuwin Current, and to shed light on its dynamics. Coastal wind data were collected at several locations, and CTD sections were made out from the shelf at selected latitudes (Fig. 1). Prior to LUCIE, there were few detailed observations in the Leeuwin Current and the only previous long-term direct current observations were on the North West Shelf in 1982–83 (Holloway and Nye 1985) and at midshelf offshore from Dongara during 1973–75 (Cresswell et al. 1989). There were no long-term current meter measurements in the core of the Leeuwin Current and only a few hydrographic sections across the current.

The purpose of this paper is to present a more complete description of the Leeuwin Current, based on the current meter moorings and CTD surveys made during LUCIE. The structure and the seasonal variability will be addressed and discussed with reference to the alongshore pressure gradient and coastal winds. Some of the conceptual models, which form the basis of theoretical and numerical models, will be compared with the evidence from LUCIE.

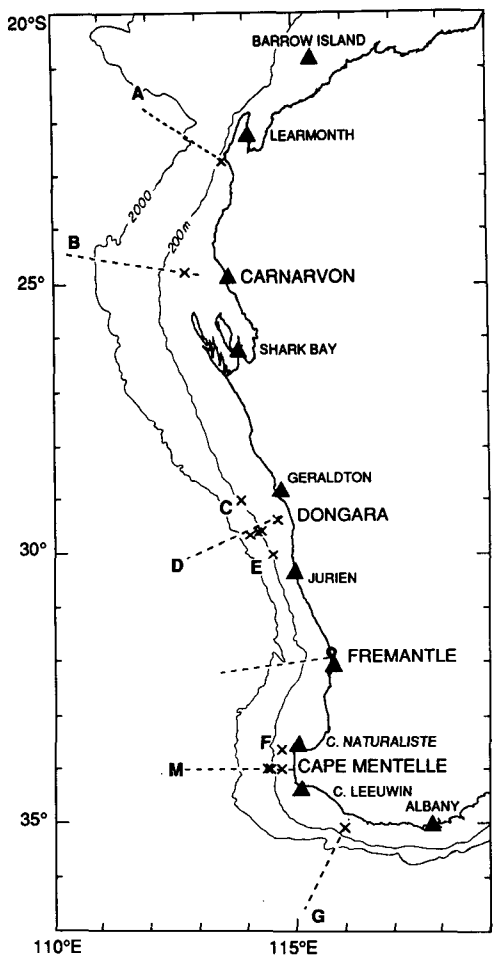

FIG. 1. Map showing the location of current meter moorings (x), CTD sections (dashed lines), coastal meterological stations (triangles) and the tide gage at Fremantle (open circle).

2. Data collection

a. Current observations

The LUCIE current meter moorings were deployed in an alongshore array along the shelf-edge and two across-shelf arrays spanning the upper continental slope (Fig. 1). Some moorings were in place continuously from September 1986 to August 1987, others were recovered and redeployed in February 1987, and still others were in place only from February to August 1987. Most of the instruments were Aanderaa current meters on moorings with subsurface flotation, but a few Neil Brown current meters and one General Oceanics S4 current meter were deployed with surface meteorological buoys to measure near-surface currents. Successive records from the same nominal location and depth were joined by means of a predictive filter based on the spectral characteristics of the data on either side of the gap; all gaps so treated were less than 175 hours (i.e., less than 3% of the complete record length). The processed hourly or half-hourly current data low-pass filtered (half-power at 0.6 cpd) and resolved into local onshore and alongshore coordinates. To examine the qualitative behavior of the currents at locations where direction data only were available, missing speed data were replaced with a constant value before low-pass filtering; such speed gaps are explicitly identified in the appropriate figure caption. Details of the current meter array, the data processing and the data quality are given in Boland et al. (1988).

The alongshore array, in place from September 1986 to August 1987, consisted of seven moorings (designated A2, B2, C2, D2, E2, F2 and G2 from north to south, with particular current meters designated by appending a slash and the instrument depth). Each mooring had an Aanderaa current meter 15 m above the bottom and subsurface flotation. All of the moorings were near the shelf-edge, in water depths between 60 and 120 m (118, 80, 61, 107, 85, 75 and 76 m, at A2, B2, C2, D2, E2, F2 and G2, respectively).

One cross-shelf array of five moorings was deployed across the continental shelf and upper slope off Dongara at 29.5°S in September 1986, replaced in February 1987 and recovered in August 1987. During both periods, there were four subsurface moorings: D1 over the 53 m isobath (midshelf), D2 over the 107 m isobath at the shelf-break, and D3 and D4 over the 300 and 700 m isobaths on the upper slope. A fifth mooring, DM, with surface flotation and and meteorological sensors, was installed over the 85 m isobath, just inshore from D2, to measure the near-surface currents and wind. During the first installation, there was severe rotor fouling at D2/48 after November, and the DM mooring broke loose in early November; during the second, D1/28 and DM/23 failed completely, D3/258 yielded no speed data, and portions of D4/75 data are of doubtful quality. Off Dongara, isobaths are oriented along 150°–330°T; onshore and alongshore components of the current are toward 060° and 330°T, respectively.

A second cross-shelf array of four moorings was deployed off Cape Mentelle at 34°S between February and August 1987. There were three subsurface moorings: M2 over the outer shelf (water depth of 116 m), M3 just seaward of the shelf-break (198 m) and M4 over the 700 m isobath. A surface mooring with meteorological sensors, MM (water depth 186 m, adjacent to M3), broke its anchor chain and began to drift in late May. All of the isobaths at this latitude were directed approximately north–south, so onshore and alongshore components of the current are directed toward 090° and 000°T, respectively.

b. Hydrographic observations

Hydrographic observations were made during the mooring deployment and recovery cruises (September 1986, February 1987, August 1987) and two additional cruises (March 1987 and June 1987). On each cruise, CTD observations (using a Neil Brown Mk III CTD) were made along sections extending across the continental margin at the latitudes of most of the shelf-break moorings, with individual sections completed within 36 hours.

c. Meterological and sea level observations

The meteorological observations gathered during LUCIE are described by Forbes and Morrow (1989). In this paper we use the coastal winds recorded for the Australian Bureau of Meteorology (BoM) by local observers at nine locations, extending from Barrow Island on the North West Shelf to Albany on the south coast (Fig. 1), and hourly data from the Fremantle Port Authority. The BoM stations at Learmonth, Carnarvon, Geraldton and Albany recorded winds every three hours, but the others recorded the wind only at 0900 and 1500 local time. All data have been filtered to suppress variability at periods less than 1.5 days. Except for the most northern (Barrow Island and Learmonth) and southern (Albany) BoM stations, where the mean and principal axes directions persistently differed from north, the onshore/alongshore orthogonal axes used are eastward/northward (090°T/000°T). CSIRO meteorological buoys moored near the shelf-edge at 29.5° and 34°S provided vector-averaged hourly wind data during February-April and February-May 1987, respectively. The low-passed data from these shorter records agreed well with data from the coastal BoM stations, providing confidence in the latter. For example, during the 58 days of common record, the equatorward component of the wind at the Carnarvon BoM station (25°S) had a mean and standard deviation of 4.1 ± 2.9 m s^{-1} compared to 3.5 ± 3.4 m s^{-1} at the meteorological buoy off Dongara (29.5°S); the correlation coefficient was 0.7 (significance level >99%). Wind stresses were computed by Forbes and Morrow (1989) assuming neutral stability. Hourly tide gage data from Fremantle, provided by the Flinders Institute of Atmospheric and Marine Sciences, were filtered in the same manner as the current meter data. The atmospheric pressure data from the Cape Leeuwin BoM meteorological station were added to the sea level data to give total subsurface pressure (or adjusted sea level).

3. Winds

During LUCIE, the winds along the west coast of Australia were equatorward in the record means at all locations except Albany, but there is a clear seasonality (Fig. 2). The winds are persistently equatorward (i.e., upwelling favorable) during the austral spring and summer (October to March) with typical speeds of 5–10 m s^{-1}. During March to mid-May the winds are more variable in speed and direction but are still equatorward on average. In the late fall and winter (May to August) there is a distinct gradient along the coast: winds from the northeast at Barrow Island (21°S), variable winds between 22° and 30°S, and strong rotary variations south of 30°S, which reflect the passage of lows near Cape Leeuwin (Cresswell et al. 1989). This description of the winds is consistent with the classic wind atlas for the region (KNMI 1949), indicating that the winds during LUCIE were not anomalous.

Table 1 gives the mean and variance of the alongshore component of the wind stress for the wind records shown in Fig. 2. The statistics are given for three 72-day periods, which are representative of the different "seasons" of the wind described above, and for the longest common period (325 days) for most current meters in the main cross-shelf array off Dongara (29.5°S).

The wind velocity time series (Fig. 2) show a great deal of coherence along the coast, on both the seasonal and synoptic time-scales, with little phase lag. One empirical orthogonal mode represents 60% of the variance in the alongshore component of the winds in Fig. 2,

TABLE 1. Means and standard deviations of the alongshore wind stress (dyn cm^{-2}) for the three 72-day periods: 2 Nov to 13 Jan (a), 1 Mar to 12 May (b), and 20 May to 31 Jul (c), and for the 325-day period from 18 Sep to 8 Aug (d). Also shown is the orientation of the positive alongshore component at each location.

Location	Direction (°T)	Means				Standard deviations			
		(a)	(b)	(c)	(d)	(a)	(b)	(c)	(d)
Barrow Is	045	0.57	0.08	−0.53	0.11	0.42	0.39	0.63	0.67
Learmouth	020	0.66	0.19	0.01	0.33	0.33	0.26	0.17	0.40
Carnarvon	000	0.84	0.32	0.08	0.50	0.39	0.36	0.20	0.48
Shark Bay	000	0.74	0.21	−0.03	0.37	0.13	0.28	0.10	0.44
Geraldton	000	0.35	0.09	−0.06	0.20	0.35	0.24	0.14	0.35
Jurien	000	0.50	0.13	−0.07	0.28	0.30	0.46	0.33	0.49
Fremantle	000	0.54	0.06	0.07	0.22	0.52	0.46	0.62	0.59
C. Naturaliste	000	0.64	0.22	0.39	0.38	0.54	0.58	1.00	0.72
C. Leeuwin	000	0.66	0.23	0.63	0.31	0.51	0.87	0.84	0.75
Albany	270	0.04	−0.09	−0.19	−0.09	0.48	0.45	0.39	0.44

and accounts for more than 50% of the variance at each site except Albany. Since the winds are correlated along the central coast, it is both convenient and possible to choose a single station as representative. We have chosen Carnarvon (25°S) since it is upstream (in the shelf wave sense) of the major current meter arrays and has both a strong mean and semimajor axis of variability, with directions within a few degrees of north. The alongshore component of the wind at Carnarvon has maximum correlation at 0 lag ($C > 0.6$) with the alongshore component of the winds at the locations of the other frequently sampled wind records: Learmonth (22°S), Geraldton (29°S) and Fremantle (32°S). The Carnarvon wind is also better correlated than the other wind records with the current data from the main array at 29.5°S. The variance spectrum for the alongshore component of the Carnarvon wind (Fig. 3) shows two major peaks: the "seasonal" band (60–325 days) and the "synoptic" band (6–12 days). In the 6–12 day band, the alongshore component of the

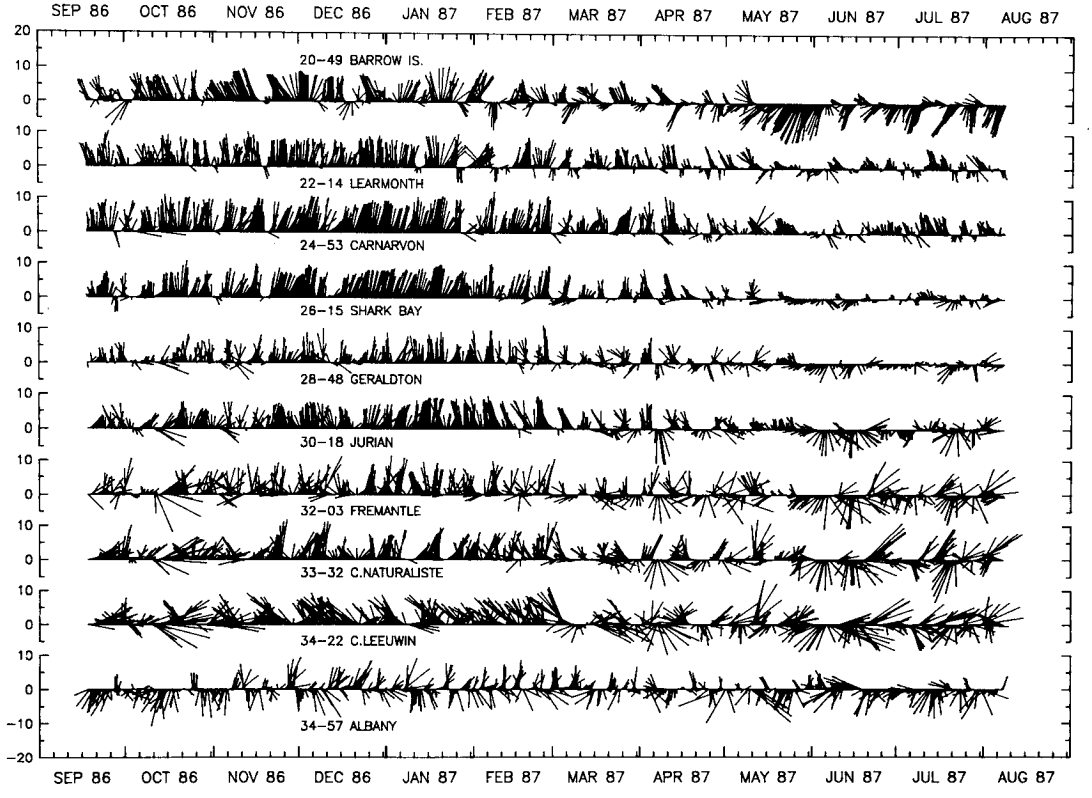

FIG. 2. Time series of the wind velocity (m s^{-1}) at 10 locations between 20° and 35°S. Vectors at Barrow, Learmonth, and Albany are relative to the local alongshore direction of 045°, 020°, and 270°T, respectively; at all other locations the vectors are relative to true north. The latitudes in degrees and minutes are listed for each location.

wind is highly coherent and in phase all along the coast. In general, the characteristics of the Western Australian coastal winds are similar to those along the ocean's other eastern boundaries: upwelling-favorable with increased variability at higher latitudes.

The time series of adjusted sea level at Fremantle is shown in Fig. 4; an annual cycle dominates with minimum sea level in spring and early summer and maximum sea level in late autumn and winter. The long-term records of monthly sea level at Fremantle show similar behavior but, during LUCIE, the monthly mean sea levels at Fremantle were lower than the 37-year means, and anomalously low (by about 0.1 m) during the austral summer resulting in a greater range than usual (Alan Pearce, personal communication). The variance spectrum for the sea level is shown in Fig. 3: The annual cycle is contained in the 60–325 day band and is dominant. The other pronounced peak is the 6–10 day band, which is coherent with the "synoptic" band of the wind.

4. Structure of the alongshore flow at 29.5°S and 34°S

a. Currents at 29.5°S

All of the low-passed current records from the Dongara array are shown in Fig. 4 (and some statistics for these records are given in Table 2). On the shelf (D1), the mean currents were northwards during summer but became progressively more southward from February to July. At the shelf-edge (D2), the currents were very coherent through the water column. There was a burst of strong southward flow in November but the maximum southward flow, up to 75 cm s^{-1}, occurred during the April/May period, and from late April to the end of the record, the strength of the southward current decreased. The strongest currents were observed at D3, where poleward velocities often exceeded 50 cm s^{-1} (and on one occasion reached 100 cm s^{-1}), particularly between mid-February and late May. At the most offshore mooring (D4), the currents were much more variable in speed and direction with the most consistent southward flow at D4/75 and D4/125 from March through May. At D4/250 and D4/450, the flow is predominantly northward and strongest from October to January. Only during December–January did the Leeuwin Current appear to be absent or very weak. The geostrophic currents computed from the hydrographic survey in late January and early February, which extended much farther seaward than the current meter mooring array, show that the Leeuwin Current had weakened rather than migrated offshore (Figs. 10 and 15, discussed later in this paper).

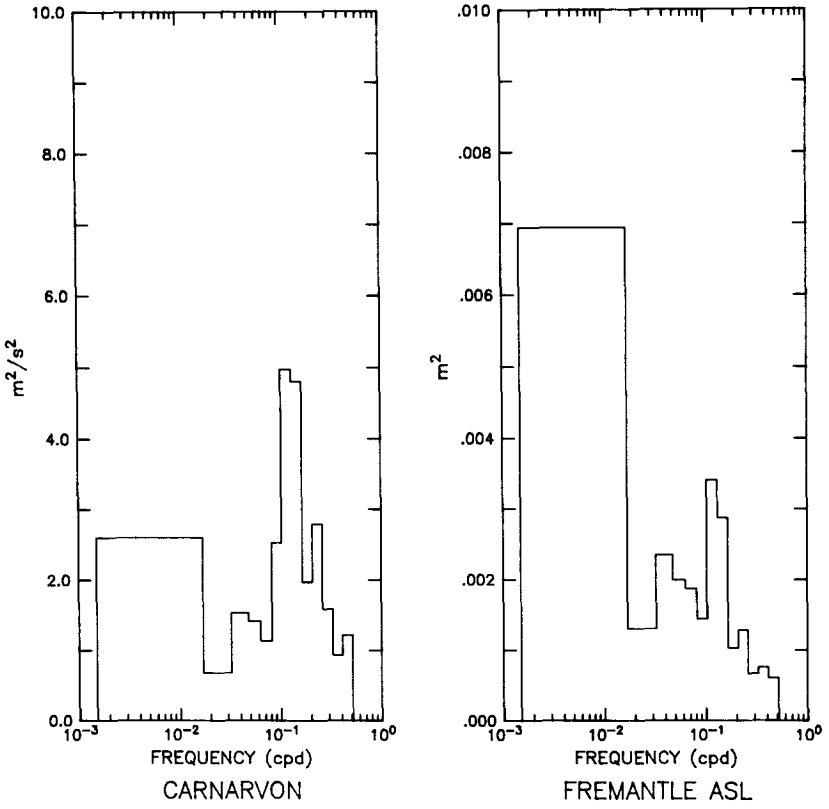

FIG. 3. Variance spectrum for the wind at Carnarvon, and for the adjusted sea level at Fremantle, calculated from 12-hourly data for the 325 day period beginning 18 September. Spectral estimates have at least 10 degrees of freedom.

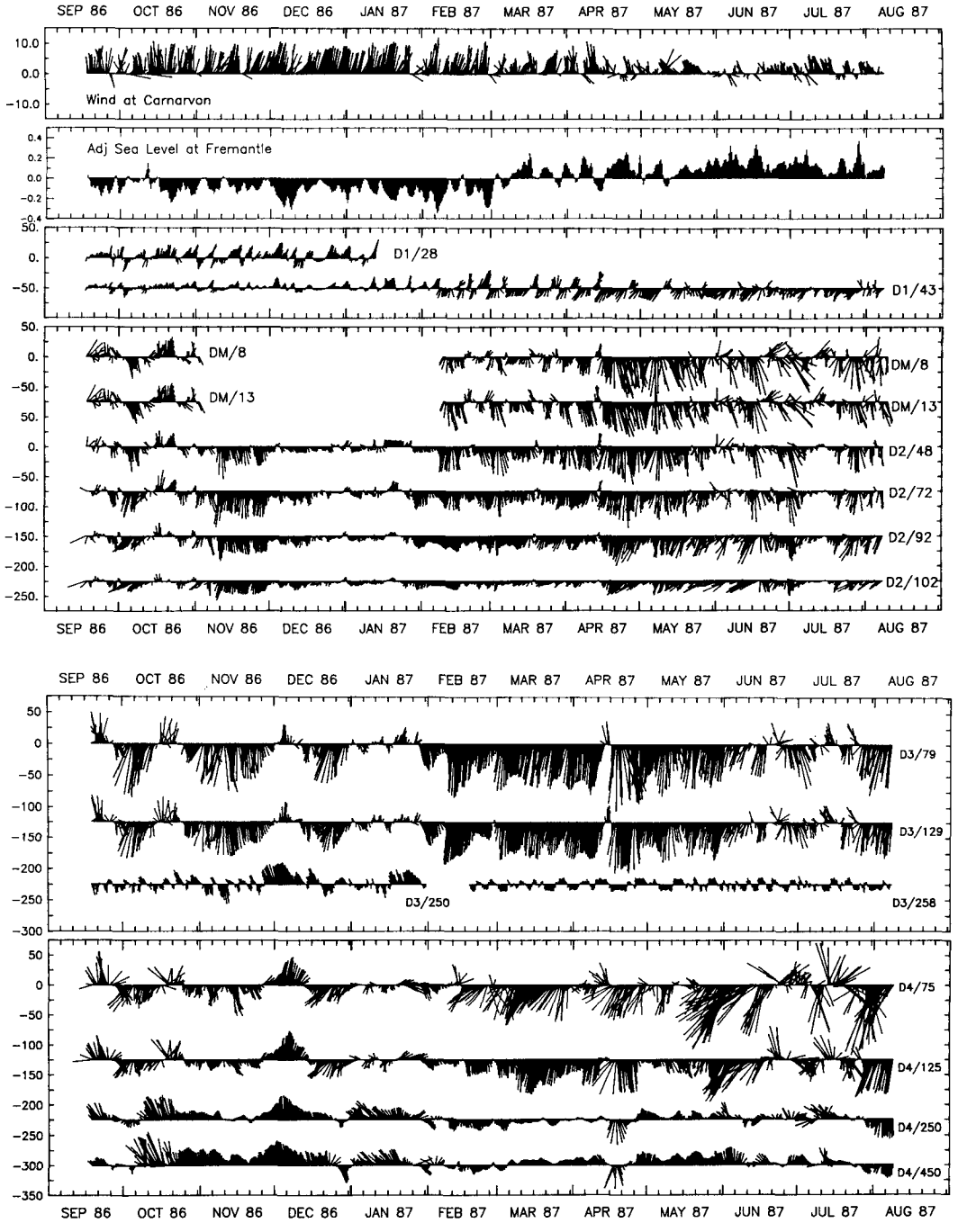

FIG. 4. Time-series of low-passed current vectors (cm s^{-1} relative to 330°T) measured at moorings of the Dongara array at 29.5°S: (a) D1, D2, and DM, and (b) D3 and D4. Note that good-quality records from Periods 1 and 2 were joined, and missing speed data (between 30 November and 17 February at D2/48, and from February through August at D3/258) were replaced with constant speeds of 10 cm s^{-1}, before the records were low-pass filtered. The low-passed wind (m s^{-1}) at Carnarvon and the adjusted sea level (m) at Fremantle are shown at the top.

To examine the structure of the Leeuwin Current over the shelf and upper slope off Dongara at 29.5°S, we show the statistics of the alongshore component of the currents (Figs. 5 and 6) for the longest possible common time period (325 days from 18 September 1986 to 9 August 1987), and for the three 72-day periods representing different "seasons" of the winds. The 325-day means (Fig. 5) show a shallow poleward current with a maximum of about 30 cm s^{-1} just seaward of the shelf break; below 250 m there is an equatorward

TABLE 2. Statistics of the current u, v (cm s^{-1}) and temperature T (°C) data from the Dongara array. For each record, the table shows the beginning and end dates of the low-passed data record; the number (N) of 12-hourly values; the means and standard deviations of temperature and of the onshore and alongshore components of the current; the percent variance (%) explained by the first empirical orthogonal mode of the alongshore current for the 325-day period 18 Sep–8 Aug (which excludes DM, D1/28, D3/250); and the direction of the vector mean (θ_m) and the orientation of the principal axis (θ_{pa}) of the current in degrees true.

	Depth (m)	N	Means			Standard deviation			%	θ_m	θ_{pa}	Record length
			T	u	v	T	u	v				
D1	28	236	19.56	2.4	4.7	0.82	4.0	10.8	—	358	347	17 Sep–13 Jan
	43	650	20.41	−2.0	−2.4	1.13	6.3	10.8	12	190	176	17 Sep–8 Aug
DM	8	364	22.51	2.2	−17.0	0.79	10.0	21.0	—	143	145	9 Feb–10 Aug
	13	364	22.28	4.0	−16.2	0.78	8.4	18.9	—	136	140	9 Feb–10 Aug
D2	48	650	20.96	1.6	−13.7	1.26	4.9	16.3	48	143	151	17 Sep–8 Aug
	72	650	20.69	−0.4	−15.1	1.31	4.8	14.3	40	152	153	17 Sep–8 Aug
	92	650	20.50	−3.5	−14.2	1.28	7.1	11.0	46	164	166	17 Sep–8 Aug
	102	650	20.35	−6.3	−7.8	1.20	9.6	6.6	25	189	222	17 Sep–8 Aug
D3	79	649	20.33	−2.4	−29.9	1.20	8.1	29.8	83	154	154	18 Sep–8 Aug
	129	649	19.41	−1.5	−23.0	1.24	6.2	24.0	85	154	153	18 Sep–8 Aug
	250	271	19.28	−3.8	−7.1	0.47	6.4	7.6	—	178	180	17 Sep–31 Jan
D4	75	651	20.16	−8.1	−19.1	1.22	24.2	31.4	56	173	181	18 Sep–9 Aug
	125	651	18.73	−2.6	−14.1	1.45	13.3	21.9	68	160	166	18 Sep–9 Aug
	250	651	14.56	−2.5	4.8	0.98	8.6	12.8	51	302	310	18 Sep–9 Aug
	450	651	9.37	−2.4	9.2	0.28	7.5	13.4	16	316	312	18 Sep–9 Aug

undercurrent with a maximum of 9 cm s^{-1} at a depth of 450 m. Both the mean poleward surface current and the equatorward undercurrent persist through each of the three 72-day periods. The surface poleward current is weakest and shallowest (and the equatorward undercurrent is strongest, at 15 cm s^{-1}) during the No-

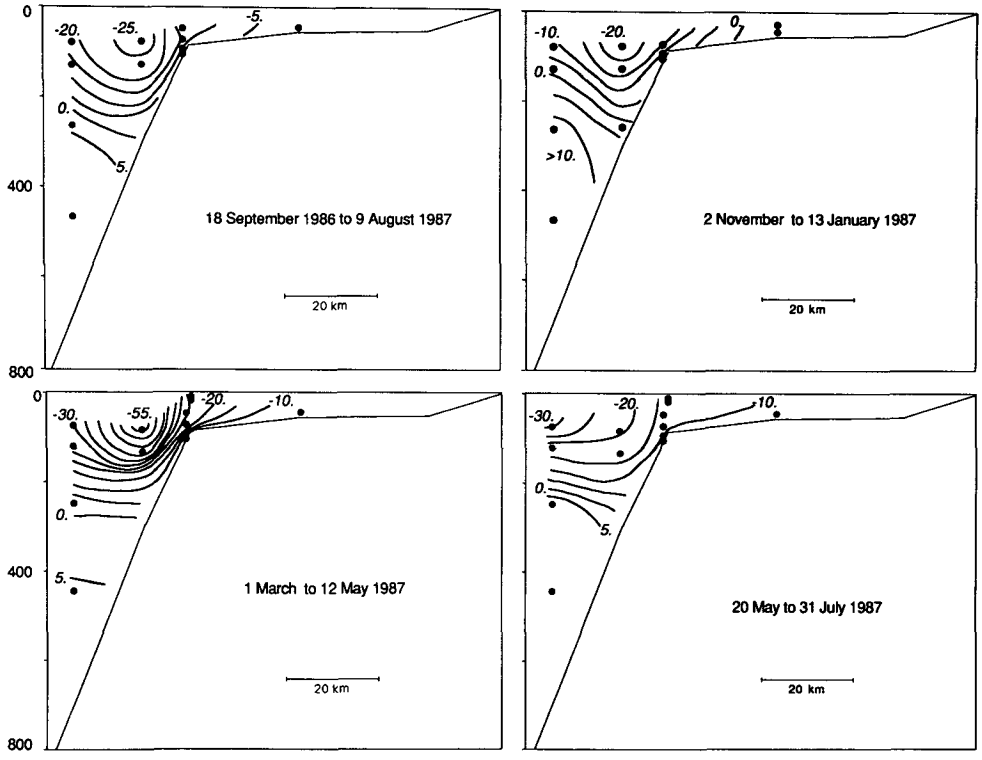

FIG. 5. The cross-shelf structure of the mean alongshore current off Dongara at 29.5°S, for the longest common (325-day) period and for three 72-day periods in different seasons. Units are cm s^{-1} with negative sign indicating poleward flow.

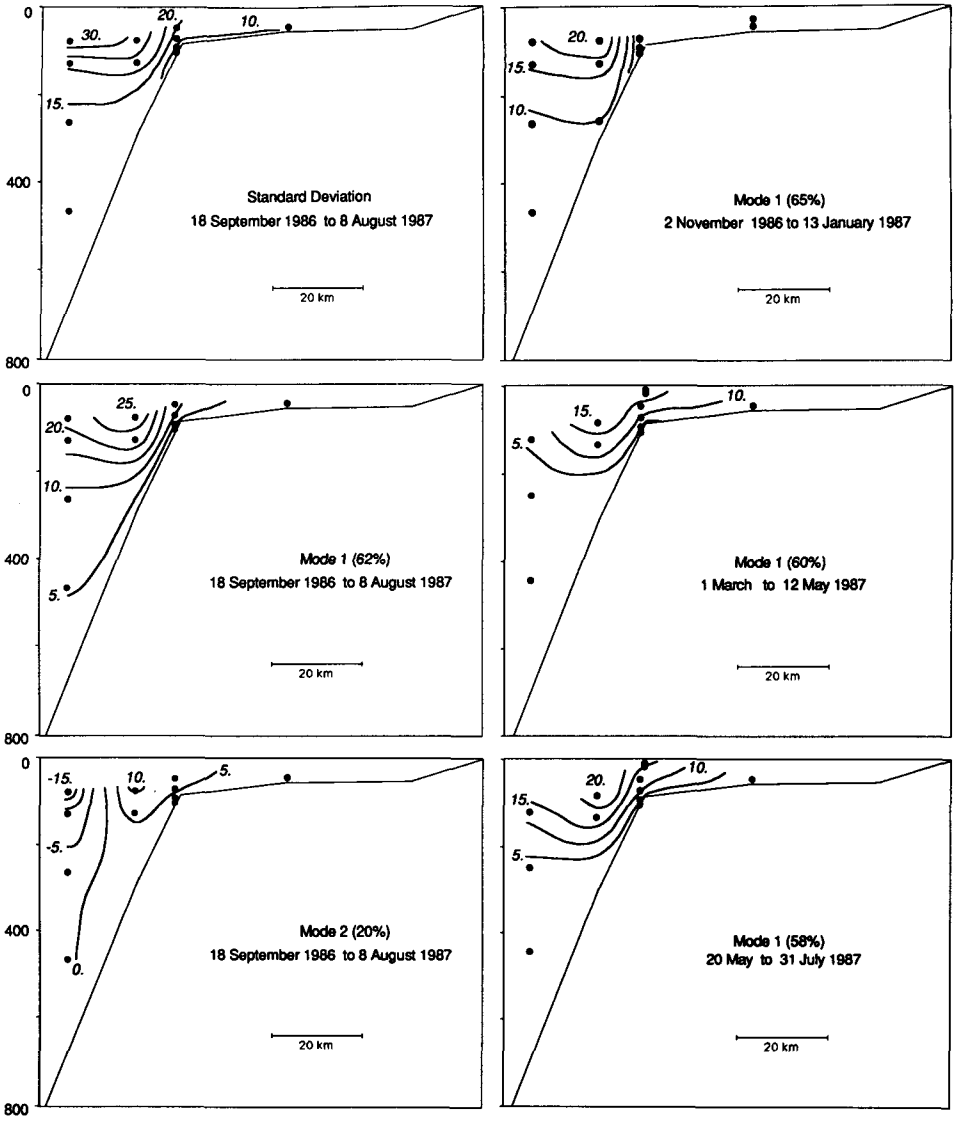

FIG. 6. The cross-shelf structure of the current variability off Dongara at 29.5°S: The standard deviation and the first two empirical modes for the 325-day common period, and the first mode for each 72-day period. Units are cm s^{-1}.

vember–January period of strongest equatorward (upwelling-favorable) winds. The poleward surface current was most intense (greater than 55 cm s^{-1}) and penetrated the deepest during the March–May period when winds were most variable. During the May–July period when winds were weak or poleward (unfavorable for upwelling), the surface flow was still poleward, but its core was no longer confined to the upper slope. Instead, the poleward flow over the upper slope was weaker, broader and shallower (confined to the upper 200 m). In each period, the mean current was much stronger over the slope than over the shelf.

Empirical orthogonal functions of the alongshore current at 29.5°S were computed by calculating the eigenvectors of the covariance matrix with the means removed; the eigenvector components were scaled by the square root of the corresponding eigenvalue to give units of cm s^{-1}. For the 325-day period and all three 72-day periods, the first mode (Fig. 6) accounts for about 60% of the alongshore current variance measured by the current meters in the cross-shelf array. (The percent of the variance at each current meter which is explained by the first mode is shown in Table 2 for the 325-day period.) In each period, the first mode represents fluctuations that have the same sign at all depths and mooring sites; the amplitude is largest near the surface just seaward of the shelf-break, and is small over the midshelf and in the deep water over the slope. The position of the maximum amplitude coincides with the core of the mean poleward flow (compare

Figs. 5 and 6); one has the impression that the first mode represents variations in the strength of the Leeuwin Current. The second empirical orthogonal mode for the complete record (Fig. 6) and for each period accounts for only about 20% of the variance and changes sign between midshelf and the offshore mooring; small on/offshore migrations in the position of the core of the Leeuwin Current could result in this pattern. Eddies, which are common in this region (Cresswell and Golding 1980; Griffiths and Pearce 1985), might produce a similar pattern if they approach the upper slope. However, neither eddies nor offshore migrations of the Leeuwin Current were resolved with the LUCIE current meter array due to its limited offshore extent. The equatorward undercurrent below 300 m was also not adequately defined by either the current meter array or the hydrographic surveys.

The variance spectra computed using the 325-day common period are shown in Fig. 7 for a subset of the cross-shelf array. The currents over the slope (D3 and D4) have most of their variance at periods > 12 days, while at midshelf (D1) most of the variance is at periods < 12 days. The shelf edge (D2) has a more uniform distribution of variance with frequency. The Fremantle sea level and the alongshore currents have a 180° phase difference (within statistical error) for all periods > 4 days, which is consistent with geostrophy, but the coherence magnitudes vary greatly. The coherence of sea level with D1 is highly significant (>99% level) for all periods > 5 days, but with D4 only for periods > 30 days. The variance in the alongshore current over the midshelf (D1) is very highly coherent (>99% level) with the Carnarvon wind in both the 6–12 and 30–325 day bands, with the wind leading by about 1 day, and significantly coherent (>90% level) at all periods except the 15–30 day band of low variance. One concludes that the currents inshore of the shelf-edge are forced directly by the coastal wind. The variance in the currents at D2, D3 and D4 was also coherent with the wind in the 6–10 day band (at the 95% level, currents lagging the wind by 2 ± 1 days), but not as coherent (significance levels > 80%) with the wind in the 30–365 day band; there were no other periods at which the coherence was generally significant. The 6–12 day band is the most energetic band for the wind (Fig. 3); the high coherence of the currents with the wind is not surprising but, because of the large alongshore coherence scale (and the small phase differences) of the winds, it is difficult to determine the relative importance of local and remote forcing by the wind.

b. Currents at 34°S

For more than six months, current measurements at the across-shelf array off Cape Mentelle at 34°S (Table 3) were made concurrently with those off Dongara at 29.5°S. The bottom profiles are distinctly different at the two latitudes (the outer edge of the shelf is much

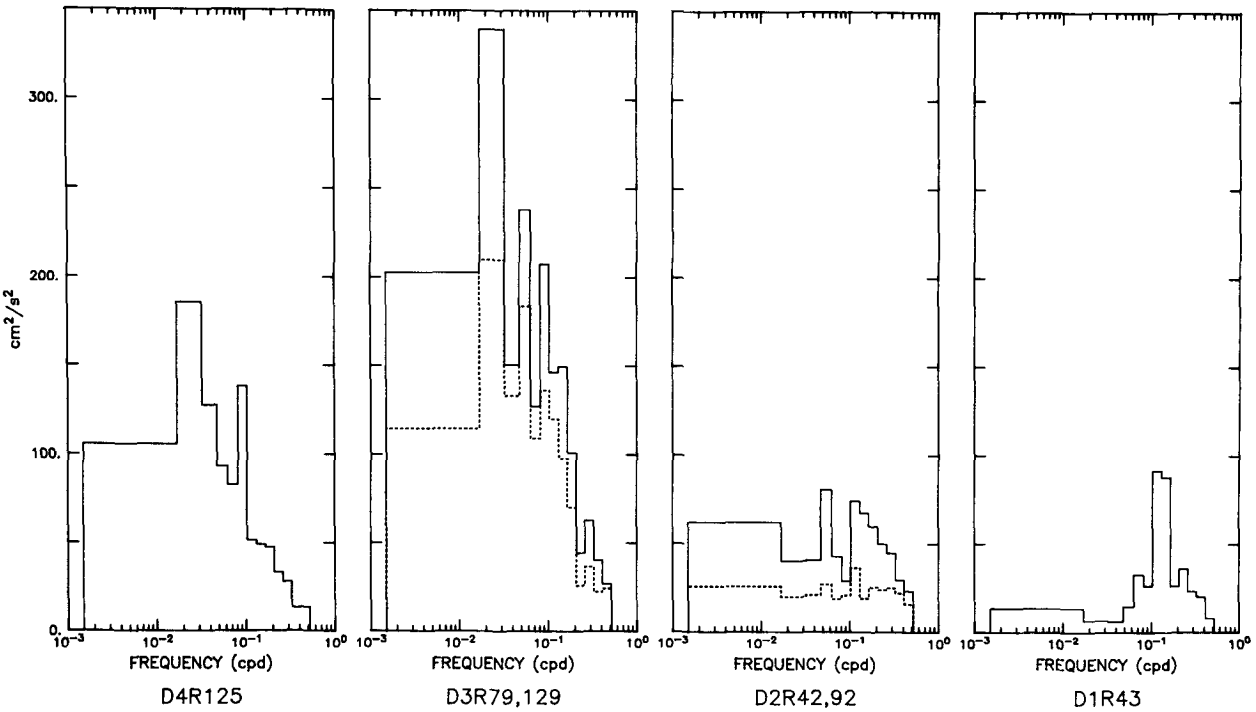

FIG. 7. Variance spectra for selected current records off Dongara at 29.5°S, calculated from 12-hourly data points for the 325 day period beginning 18 September. The deeper current spectra are dashed. Spectral estimates have at least 10 degrees of freedom.

TABLE 3. Means and standard deviations of the current and temperature, and the direction of the mean and principal axis, and the beginning and end dates of the current records from the Mentelle array at 34°S.

	Depth (m)	N	Means T	Means u	Means v	Standard Deviation T	Standard Deviation u	Standard Deviation v	θ_m	θ_{pa}	Record length
M2	76	338	19.95	2.3	−13.7	1.07	4.6	15.6	171	170	12 Feb–31 Jul
M3	171	337	17.67	−7.5	−16.2	1.76	6.5	14.1	205	186	13 Feb–31 Jul
MM	8	178	21.20	−4.0	−22.8	0.88	9.2	20.4	190	179	12 Feb–12 May
	43	214	20.53	0.2	−28.8	0.96	12.0	22.6	180	181	12 Feb–30 May
M4	90	337	24.64	0.0	−23.8	2.58	12.7	24.0	180	182	13 Feb–31 Jul
	160	337	16.88	−0.0	−13.4	2.05	9.3	20.0	180	172	13 Feb–31 Jul
	230	336	14.41	−1.0	−3.2	1.96	6.9	20.3	197	176	13 Feb–31 Jul
	320	336	12.14	0.1	3.8	0.94	5.6	22.2	001	358	13 Feb–31 Jul

deeper and the continental slope is much steeper at 34°S), and the sampling at 34°S did not extend as far out to sea as at 29.5°S (the single slope mooring on the 700 m isobath at 34°S was only 6 km from the shelf-edge mooring). As at 29.5°S, the flow at 34°S was clearly southward on the shelf and near the surface on the slope (Fig. 8). However, there appeared to be more variability at 34°S than at 29.5°S.

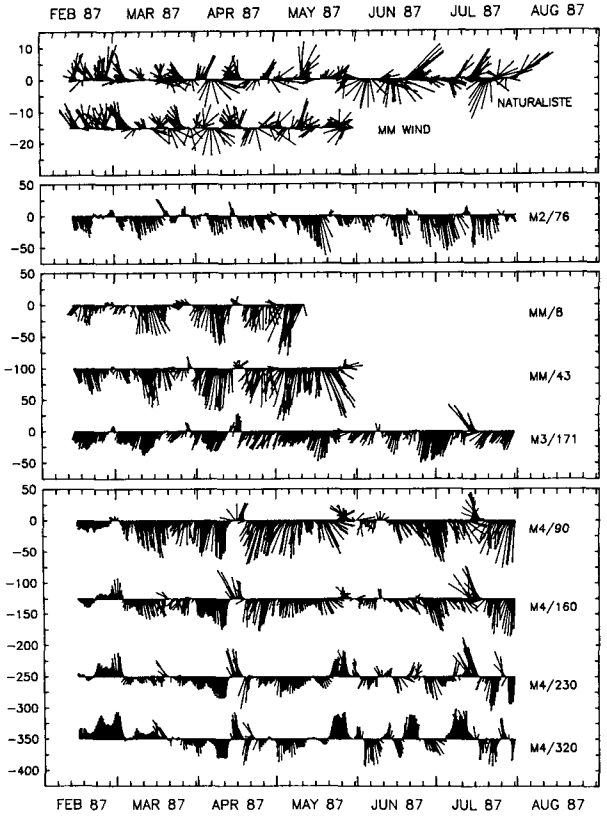

FIG. 8. Time series of low-passed current vectors (cm s^{-1} relative to 000°T) measured at moorings of the 34°S array off Cape Mentelle. Low-passed winds (m s^{-1}) at the MM-buoy and at Cape Naturaliste are shown at the top.

Means, standard deviations and empirical orthogonal modes of the alongshore flow at 34°S were calculated for the second and third 72-day periods used for the 29.5°S array. During the second period, beginning 1 March 1987, the maximum mean poleward flow occurred near the surface just seaward of the shelf break (Fig. 9); the maximum value (33 cm s^{-1}) was not as large as at 29.5°S (55 cm s^{-1}, Fig. 5) but the poleward flow did penetrate to a greater depth (to at least 320 m). No shallow data were available from the shelf-break during the third 72-day period, but the available data indicate the poleward flow had weakened, as it had at 29.5°S. The equatorward undercurrent over the slope was not observed at 34°S during the March–May period but it was present below 230 m in the May–July period.

As at 29.5°S, the current variability at 34°S was stronger over the upper slope and shelf-break than on the midshelf (Fig. 9). The amplitude of the first empirical orthogonal mode penetrates deeper at 34° than at 29.5°S (Fig. 9). As at 29.5°S, the first mode is consistent with variations in the strength of the Leeuwin Current. In both of the 72-day periods, the time series of the amplitude of the first mode at 34°S are significantly correlated ($C > 0.5$, significant at the 95% level) with the first mode at 29.5°S, the latter leading by about 1.5 days.

c. *Hydrographic observations*

The Leeuwin Current and its seasonal waxing and waning can be clearly seen in the repeated CTD sections at Dongara (Fig. 10). Except for the section made during the January–February cruise, these sections show a surface temperature maximum and a salinity minimum over the upper slope. These surface extrema indicate poleward advection, and are particularly obvious in March when the poleward flow was strongest (Fig. 4).

In early February, the isotherms in the upper 400 m were shallowest about 100 km from the coast and there was a slight downward tilt towards the coast and

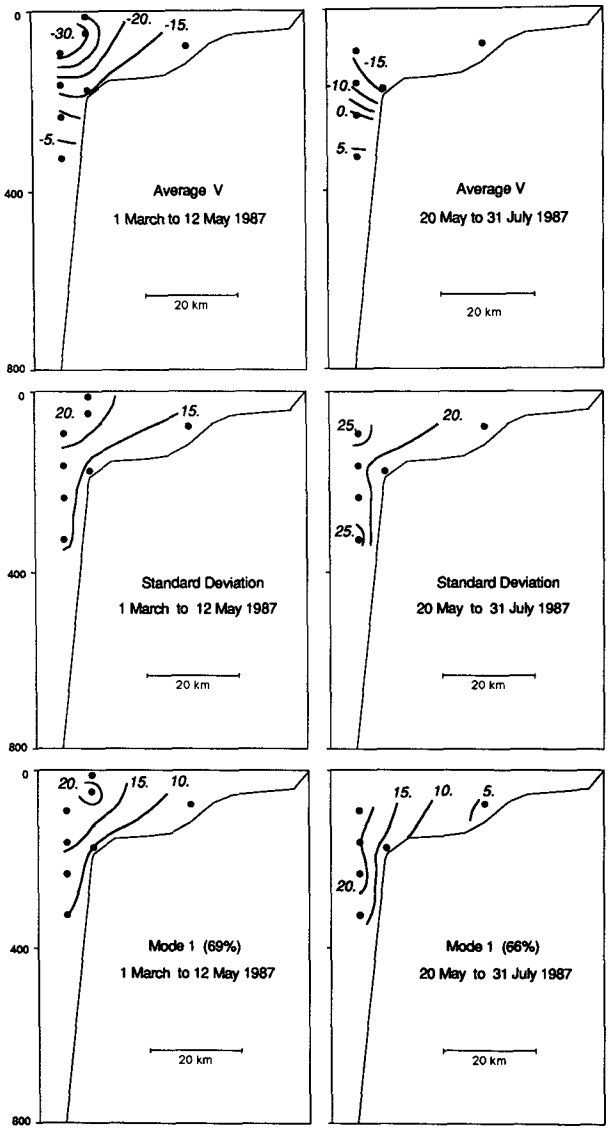

FIG. 9. The cross-shelf structure of the means, standard deviations and first mode of the alongshore component of the current off Cape Mentelle at 34°S during two of the 72-day periods also used for the Dongara Line. Units are cm s^{-1}.

offshore. The large upward tilt of the isotherms deeper than 400 m suggest equatorward flow along the slope, consistent with the deepest current meter observations in December and January (Fig. 4). The salinity section looks very similar to the temperature section and the low salinity tongue indicative of Leeuwin Current water is barely visible. By March, the current meter data (Fig. 4) indicate that the Leeuwin Current was flowing strongly, and the isotherms and isohalines tilted down sharply towards the continental slope. A core of high-temperature/low-salinity water was present just seaward of the shelf break. Below 400 m, the upward tilt of the isotherms was no longer present (Fig. 10) and the equatorward flow along the slope was very weak (Fig. 4). The high-temperature/low-salinity core continues to develop and by June the salinity at the shelf break had fallen to less than 35.4, compared to 35.8 in February. Despite it being winter, the southward advection maintained the temperatures at almost the same value in June as in March. The low salinity region was marked by weak stratification down to 200 m. As in February, there was an upward tilt of the isotherms below 400 m. In August and September, the pattern is very similar to that in June except that the surface temperature has fallen by about 2°–3°C.

Geostrophic velocity sections (Fig. 10) show the offshore extent of the Leeuwin Current. Because the current meter averages (Fig. 5) show a zero-crossing in the 200–300 m depth range, we have used a reference level of 300 db. (Hamon, 1965, also used 300 db as a reference surface in this region.) These geostrophic velocity sections are consistent with the current meter observations and show the Leeuwin Current was present during all but the January–February cruise, when winds were most equatorward. By March the flow had strengthened to a maximum of 80 cm s^{-1} over the upper slope. By June, the Leeuwin Current was very strong (>100 cm s^{-1}), but the core was about 120 km from shore, well seaward of the current meter array. The maximum poleward flow observed by the current meter array shifted offshore from D3 to D4 in May, and the maximum poleward velocity at D4 occured in early June, with a strong offshore component. In August, the poleward geostrophic current was still very strong but it was confined to a smaller cross-sectional area. One year earlier in September 1986, the currents were weaker but slightly broader than during the August 1987 cruise. Transport estimates for the Leeuwin Current at 29.5°S (geostrophic velocities integrated from 0 to 300 m depth and across the Leeuwin Current, Fig. 10, Table 5) range from less than 2 Sv (Sv $\equiv 10^6$ m^3 s^{-1}) in summer (February 1987) to more than 5 Sv in autumn and in winter (March, June and August 1987) with an intermediate value in early spring (September 1986).

5. Alongshore structure

The alongshore array of shelf-break current meters consisted of eight moorings near the 80 m isobath (Table 4), including M2 which was deployed only during the latter half of LUCIE. The actual bottom depths ranged from 118 m (A2) to 61 m (C2), but all moorings were <3 km from the 80 m isobath. Except for M2, where the only current meter was 40 m from the bottom, all moorings had current meters 15 m above the bottom. At both Dongara (29.5°S) and Cape Mentelle (34°S) the shelf-edge moorings, D2 and M2, lie inshore of the core of the Leeuwin Current and show an alongshore flow about half the seaward maximum (Tables 2, 3; Figs. 5, 9). The other shelf-edge moorings

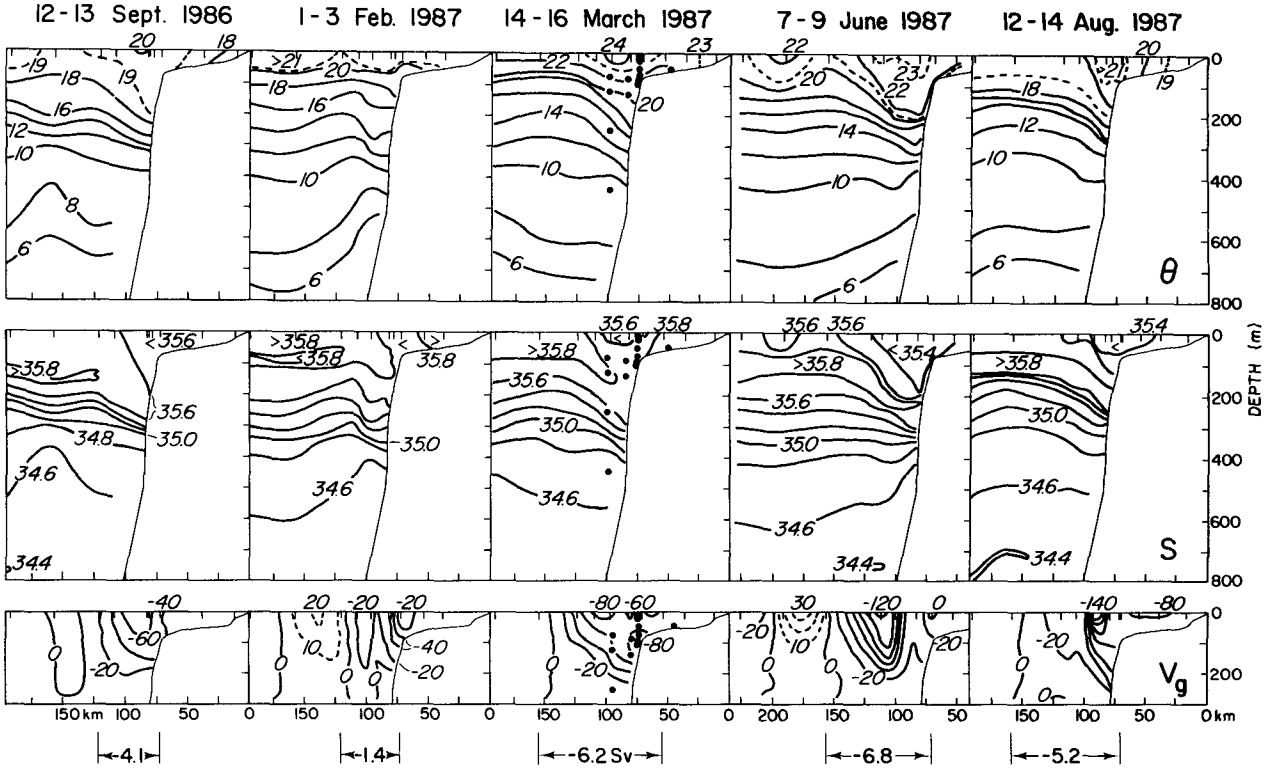

FIG. 10. Vertical sections of potential temperature, salinity, and geostrophic velocity (cm s^{-1}, relative to 300 db) off Dongara, for the five LUCIE cruises. The extrapolation technique described by Reid and Mantyla (1976) was used to calculate velocities in shallow water. The alongshore geostrophic transport (Sv) between 75 and 155 km from shore (relative to 300 db) is indicated at the bottom. Dots in the center panel show the positions of the current meters and indicate the limited offshore extent of the moored array.

were also inshore of the Leeuwin Current core defined by the geostrophic currents computed from the CTD sections. The time series of the shelf-edge currents (Fig. 11, and Fig. 8 for M2) show that the currents at all locations tend to be poleward throughout the observation period and strongest in the March–May period. The poleward currents are often in excess of 25 cm s^{-1}; only at B2, more than 50 km inshore of the 300 m isobath, is the current usually much weaker.

The variance spectra for the longest common period (258 days) for the alongshore shelf-edge array, A2 to E2, are shown in Fig. 12 with the equivalent spectra for the Carnarvon wind and Fremantle adjusted sea level. Comparing the spectra with those from the across-shelf array (Fig. 7), one sees that the shelf-edge spectra (except at D2) have most of their variance at relatively short periods and thus resemble the spectrum at mid-shelf (D1) rather than the spectra from the slope.

TABLE 4. Statistics of the current (cm s^{-1}) and temperature (°C) data from the alongshore array. For each mooring, the table shows the beginning and end dates of the low-passed data record; the number (N) of 12-hourly values; the means and standard deviations of temperature and of the onshore and alongshore components of the current; the direction of the vector mean (θ_m) and the orientation of the principal axis (θ_{pa}) of the current in degrees true; and the correlation and lag of the record compared with D2. All the correlations (except those in parentheses) are significant at the 99% level; a positive lag means the record leads D2 by the given number of days.

	Depth		Means			Standard deviation							
	(m)	N	T	u	v	T	u	v	θ_m	θ_{pa}	C	lag	Record length
A2	103	652	22.08	−0.5	−15.4	1.43	2.6	12.7	202	203	0.31	2.0	23 Sep–15 Aug
B2	65	606	22.29	0.2	−5.7	1.47	6.3	8.9	178	172	0.34	1.0	21 Sep–20 Jul
C2	46	524	20.86	1.1	−12.7	1.32	3.1	13.4	135	136	(0.21)	(0.5)	19 Sep–8 June
D2	92	650	20.50	−3.5	−14.1	1.28	7.0	11.0	164	166	—	—	17 Sep–8 Aug
E2	70	653	20.37	−6.3	−13.7	1.32	10.1	12.9	185	188	0.33	0.0	17 Sep–9 Aug
F2	58	335	20.10	−3.6	−9.5	0.98	7.2	11.9	201	202	0.30	0.0	13 Feb–30 Jul
M2	76	338	19.95	2.3	−13.7	1.07	4.6	15.6	171	170	0.29	−1.0	12 Feb–31 Jul
G2	61	254	17.60	−2.0	−6.5	0.39	3.0	9.2	137	129	(0.06)	(−0.5)	7 Sep–12 Jan

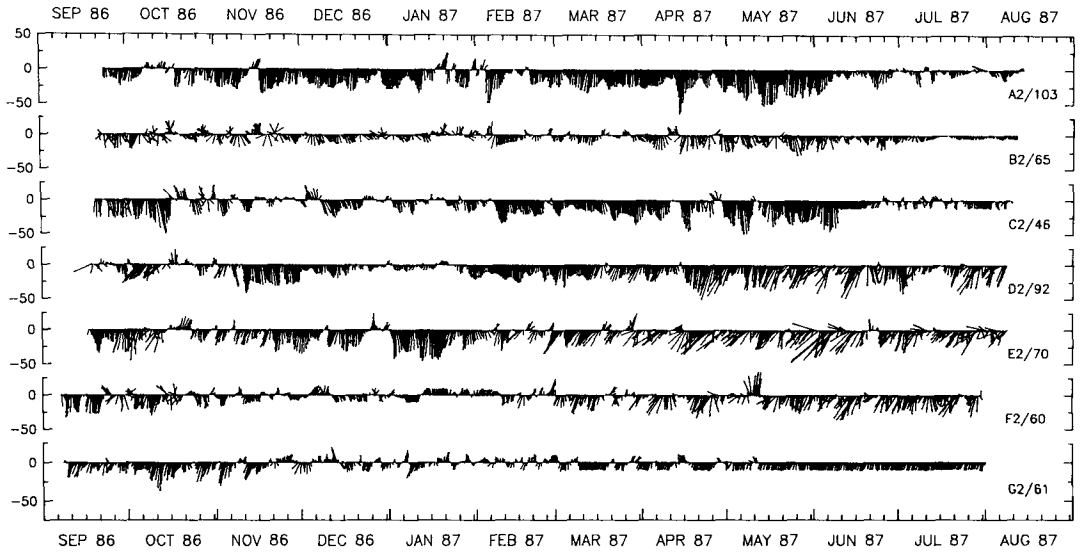

FIG. 11. Time series of low-passed current vectors 15 m above the bottom at the seven moorings along the shelf-edge between 22° and 35°S. Vectors are relative to the local alongshore direction: 020°T at A2, 000°T at B2 and F2, 320°T at C2, 340°T at E2, and 300°T at G2. Note that missing hourly speed data were replaced with constant 10 cm s^{-1} speeds over extended periods at C2 (8 Jun to 10 Aug), at F2 (12 Dec to 8 Feb) and at G2 (12 January to 1 August), before the records were low-pass filtered. Units are cm s^{-1}.

However, the band of high variance at the shelf-edge extends to longer periods (at least 20 days) than at midshelf. At all shelf-edge locations, the variance in the 6–10 day band is significantly coherent (significance levels > 95%) with the Carnarvon wind. In this band, the shelf-edge currents are also mutually coherent (significance levels generally >99%) and in phase to within the statistical uncertainty of about 1 day, leading to the conclusion that the 6–10 day fluctuations in the currents are locally forced by the coastal winds.

Extended data gaps at some locations make it difficult to compare the overall average currents, but simultaneous current measurements at seven shelf-edge moorings (including M2) were available for the 72-day period from 1 March to 12 May. The 72-day average currents show poleward flow at the shelf-edge along the entire west coast from 22° to 35°S, while average winds are equatorward and stronger along the northern coast than they are south of 27°S (Fig. 13). Variations in the average current direction reflect the local coastline and isobath orientation. The strength of the average shelf-break currents varies within a factor of three, but this variation seems to be local rather than large-scale since the largest difference occurs between neighboring moorings. The largest averages (>15 cm s^{-1} at A2, D2, E2) during this 72-day period occur at locations where the upper continental slope is steep and the shelf-break moorings are less than 10 km from the 300 m isobath. The smallest averages (<10 cm s^{-1} at B2, F2, M2) are at locations where the slope is more gradual and moorings are more than 20 km inshore of the 300 m isobath. This suggests that the Leeuwin Current core at this time of year lies over the upper slope all along the west coast, as it does off Dongara and Cape Mentelle.

CTD sections from the March cruise (Fig. 14) support this inference. Sections at 22°S (A), 25°S (B), 29.5°S (D) and 32°S (Fremantle) all have a minimum (weak at Fremantle) in the surface salinity over the inner slope, and all except B (25°S) also show a maximum in the poleward geostrophic velocity there. (At 25°S, poleward geostrophic flow is observed father offshore on 18–19 March, but the salinity distribution suggests that its predominant position is over the upper slope.) The values of surface salinity, both within the Leeuwin Current and offshore, are significantly higher along 29.5° and 32°S than they are farther north (Fig. 14); this is consistent with the eastward advection of high-salinity subtropical water between 29° and 32°S discussed by Andrews (1977). At this time of year (late summer), offshore surface waters are quite warm, and a local temperature maximum, congruent with the salinity minimum near the core of the Leeuwin Current, is observed only in the two southern sections. The axis of the poleward current seems to be "anchored" to the bottom near the 100 m isobath, tilting offshore toward the surface. Thompson (1984, 1987) attributed a similarly sloping front to cross-shelf Ekman flux and alongshore advection. The geostrophic transport of the Leeuwin Current varies little along the coast in March (Fig. 14, Table 5), ranging only from 4.1 Sv (at 22°S) to 5.3 Sv (at 29.5°S). The similarity of the 22°S section to those farther south indicates that flow along the North West Shelf augments the Leeuwin Current at

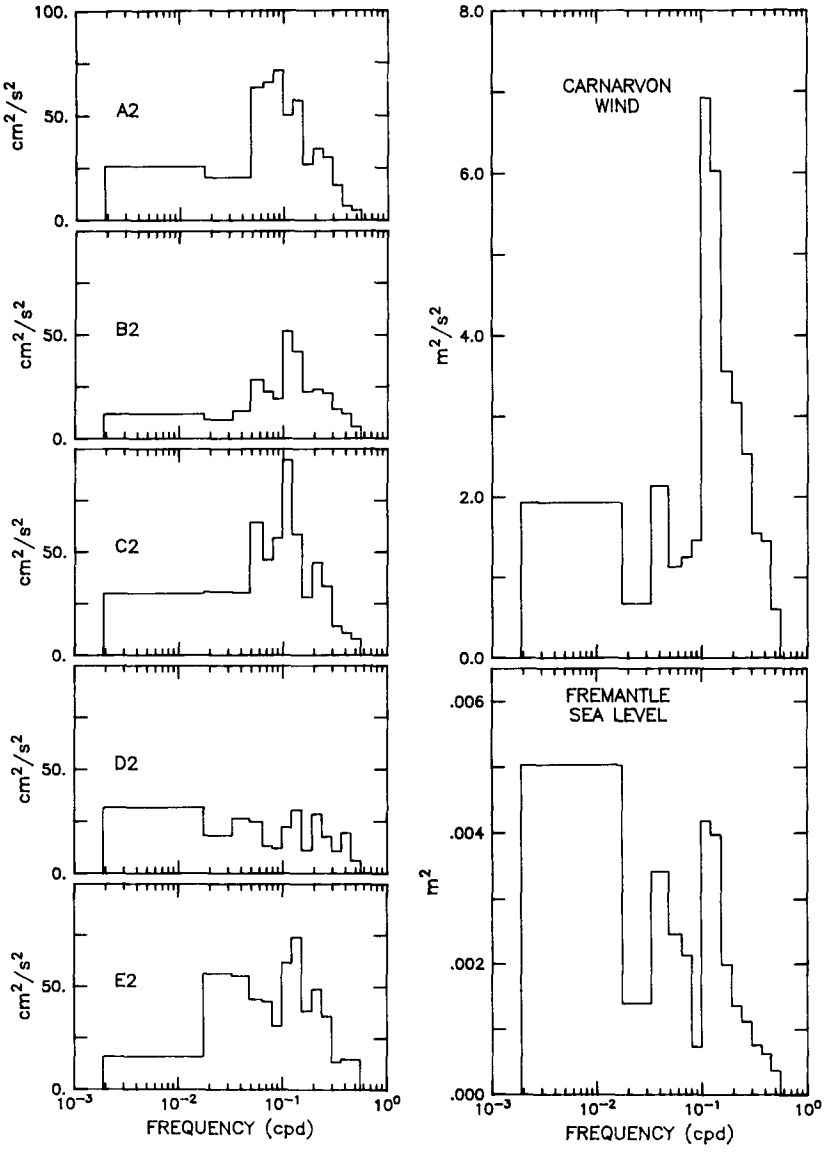

FIG. 12. Variance spectra for five shelf-break current records, calculated from 12-hourly data for the 258-day period beginning 23 September. Spectral estimates have at least 8 degrees of freedom. Comparable spectra for wind and sea level are shown at right.

this time of year; this can also be seen in the map of the surface geopotential anomaly for March (Fig. 15).

Most of the CTD sections from the August 1987 cruise, in the season when average winds are weak (Fig. 2), show a similar structure, with a salinity minimum, a temperature maximum and a poleward geostrophic velocity maximum over the upper slope (Fig. 16). The temperature contrast between the maximum at the core of the poleward current and the surface waters offshore increases downstream: from <1°C at A (25°S) to >2°C at M (34°S), and >5°C at G (35°S). Surface salinities within the current and offshore increase between 25° and 34°S, indicating onshore advection of subtropical water (Andrews 1977). Surface waters offshore at G are significantly cooler and fresher than those at D and M, while the temperature and salinity of the Leeuwin Current core remain more nearly the same. Thus, at G (and farther east along the south coast, Godfrey et al. 1986) the advective signature of the Leeuwin Current is a local maximum in both temperature and salinity over the inner slope. Only in the most northern CTD section (22°S) is there no temperature maximum, salinity extremum, or poleward flow over the upper slope; if the Leeuwin Current is present at this latitude in August, its core is about 150 km offshore. The poleward transport (>3 Sv) centered 150 km offshore is greater than the equatorward transport (1 Sv) inshore;

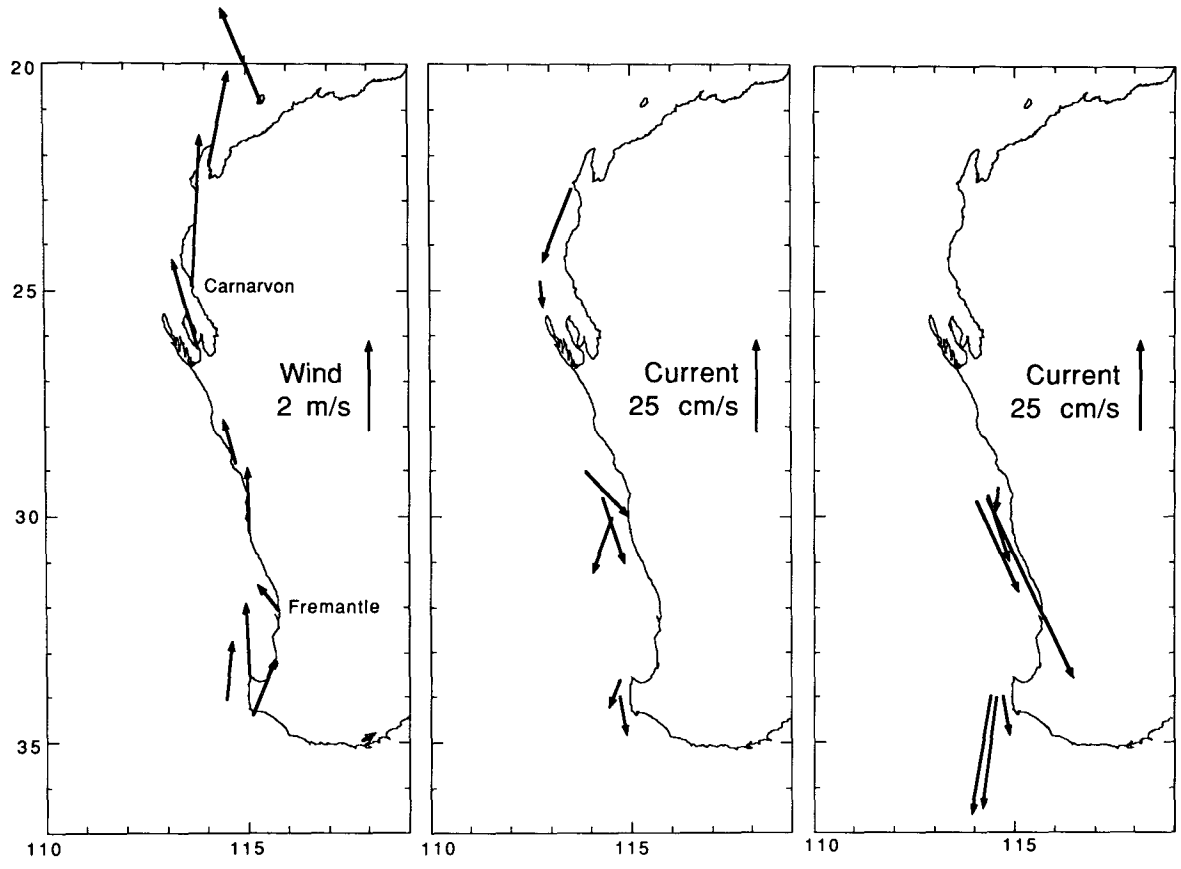

FIG. 13. Mean current and wind vectors for the 72-day period of 1 March to 12 May when the Leeuwin Current has its seasonal maximum strength. Left: winds at coastal stations and the MM buoy. Middle: currents 15 m above the bottom at the shelf-break moorings. Right: currents at the shallowest instrument which was more than 25 m below the surface on the moorings off Dongara (29.5°S) and Cape Mentelle (34°S). Scales are 2° latitude equals 2 m s^{-1} for wind and 25 cm s^{-1} for current.

the map of surface dynamic topography (Fig. 15) suggests it has an onshore component. The circulation in September 1986 was similar (Fig. 15).

We have computed the geostrophic onshore transport through the sections defined by the most offshore stations on each of the lines shown in Fig. 15 (Table 5). Throughout the year, there is significant onshore transport (relative to 300 db) between A and D, i.e., eastward transport between 22° and 30°S. The transports in September 1986 and August 1987 are in close agreement (6.5 and 6.6 Sv, respectively); the transport in March is less (4.5 Sv). The wind-driven Ekman transports through the same lines were calculated by averaging the coastal wind stress data over 36-day periods encompassing each cruise. Except in January–February, the Ekman transport is negligible in comparison with the geostrophic transport, even if the wind stress values used for computing the Ekman transport have been underestimated by a factor of two.

The alongshore transport has been computed (Table 5) through each of the cross-shelf sections, both for the entire section, which extends beyond the Leeuwin Current, and for a "subjective" estimate of the width of the Leeuwin Current (Table 5). The transport of the Leeuwin Current is fairly uniform between 25° and 34°S. Except for the low alongshore transport values in February, there is little "seasonal" variation in the alongshore transport (Table 5). The low geostrophic velocities in February are consistent with the current meter data in January (Fig. 4) although by the end of the CTD cruise (14 February) the currents are strong.

One plausible "seasonal" variation emerges from the above discussion. The late winter cruises (September 1986 and August 1987) show weaker poleward flow through A (22°S) and stronger onshore flow between A and D (22°–30°S) than the early autumn cruise (March 1987). Thus, in late winter the Leeuwin Current seems to be fed primarily by subtropical offshore surface waters. The large alongshore transport through A in March (early autumn) suggests the augmentation of the Leeuwin Current by flow from the North West Shelf region at that time. This seasonal pattern is consistent with local current measurements on the North West Shelf in 1982 and 1983 (Holloway and Nye 1985), and with the large-scale seasonal variation of

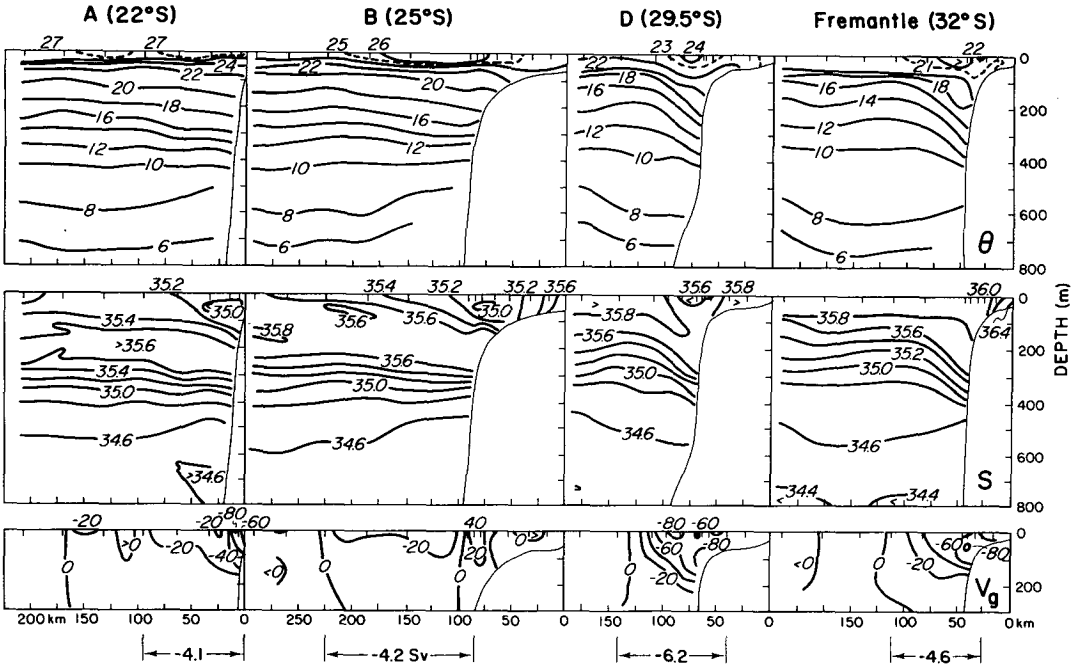

FIG. 14. Vertical sections of potential temperature, salinity, and geostrophic velocity (cm s^{-1}, relative to 300 db) at four latitudes during 12–22 March 1987. The extrapolation technique described by Reid and Mantyla (1976) was used to calculate velocities in shallow water. The alongshore geostrophic transport between indicated limits is shown at the bottom.

the hydrographic fields around Western Australia described by Godfrey and Ridgway (1985).

6. Discussion

There is general agreement that the Leeuwin Current is generated by the anomalously large (compared with other eastern boundaries of the ocean) meridional steric height gradient in the eastern South Indian Ocean: The alongshore pressure gradient overwhelms the equatorward wind stress. This was pointed out by Thompson (1984) and by Godfrey and Ridgway (1985) and used in a number of recent models (McCreary et al. 1986; Thompson 1987; Weaver and Middleton 1989; Batteen and Rutherford 1990).

The LUCIE CTD (hydrographic) cruises in September 1986, and February, March, and August 1987 had a meridional extent of at least 1000 km and provide a basis for estimating the alongshore pressure gradient. Figure 17 shows the alongshore profile of the geopotential anomaly at the first stations seaward of the 2000 m isobath; at 30°S, this station was just seaward of the edge of the Leeuwin Current and about 85 km seaward of the 100 m isobath. The geopotential anomaly (steric height) of the sea surface relative to 300 db increases to the north, indicating a tendency for onshore geostrophic flow at the surface. At deeper levels, e.g., at 450 m (the level at which the D4 mooring showed net equatorward flow), the geopotential anomaly relative to 1300 db decreases to the north, indicating weak offshore geostrophic flow at this depth. The large-scale alongshore gradient of geopotential anomaly at the sea surface changed little during LUCIE; the least squares estimate of the gradient relative to 300 db is 2.6 (±0.2) $\times 10^{-6}$ m s^{-2}. [Hamon (1965) commented on "the importance of the upper 300 m in determining the surface dynamic topography" in the region and noted that the mean dynamic topography gradient of the 300 db surface relative to a deeper surface (1750 db) is small and opposite to that of the surface (-0.5×10^{-6} m s^{-2}). In our case the slope of the 300 db surface relative to 1750 db is -0.2 (±0.2) $\times 10^{-6}$ m s^{-2}, which is essentially level, while the slope of the 450 db surface relative to 1750 db is -0.4 (±0.2) $\times 10^{-6}$ m s^{-2}, opposite to the surface slope.]

The results from LUCIE (Fig. 17) are almost identical with those presented by Hamon (1965; relative to 300 db in his Fig. 14) which were based on five "seasonal" cruises in 1962 and 1963 along 110°E between 9° and 32°S. There is little or no evidence of seasonal variability in either study. The zonal profiles of geopotential anomaly at 30°S (Fig. 17) show an increase toward the coast at the sea surface, and a slight decrease toward the coast at depth. There is considerable "seasonal" variability in the surface geopotential anomaly at stations near the shelf-edge, but even here the alongshore gradient varied little, ranging from 2.1 (±0.2) $\times 10^{-6}$ m s^{-2} in February 1987 to 2.6 (±0.4) $\times 10^{-6}$ m s^{-2} in September 1986 along the 500 m isobath.

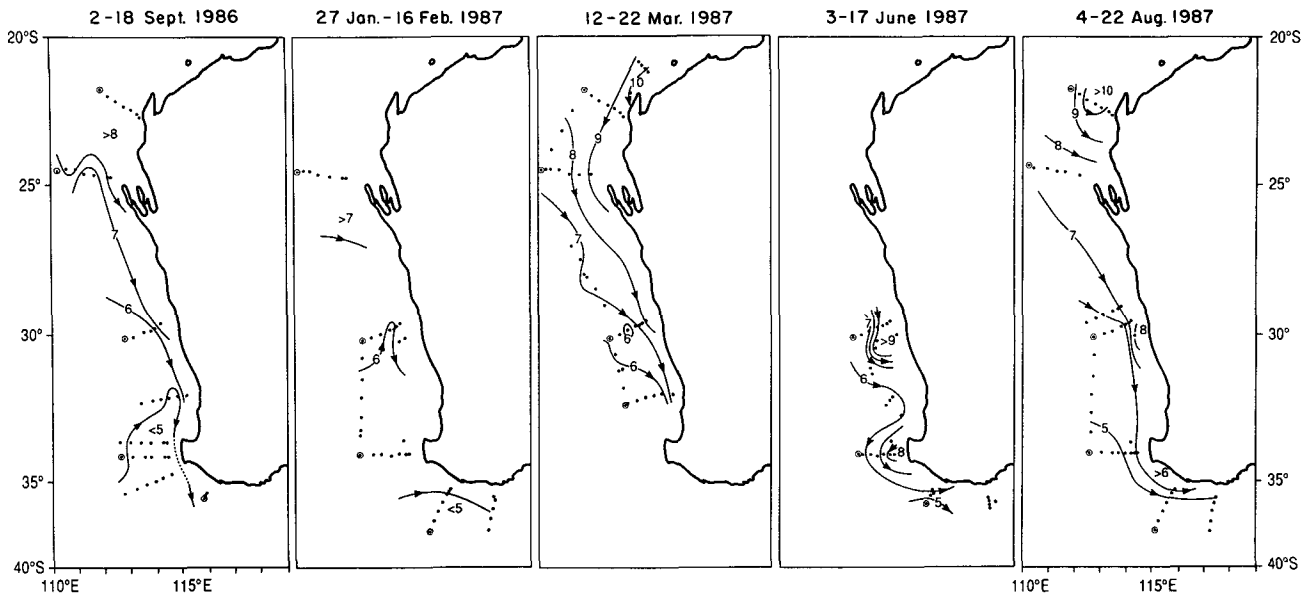

FIG. 15. Maps of the geopotential anomaly (J kg^{-1} = m^2 s^{-2}) of the sea surface relative to the 300 db surface, using only stations which sampled to at least 300 db. The contour interval of 1 m^2 s^{-2} is equivalent to 10 cm of sea surface elevation.

Given the persistent alongshore pressure gradient, is the poleward flow along the inner slope and outer shelf essential for a dynamical balance? We can test the balance suggested by Thompson (1987): The alongshore pressure gradient is balanced by the alongshore wind stress and bottom friction acting on the poleward flow, and the net onshore transport is brought to zero near the shelf-edge:

$$\int_B^0 fudz = 0$$

$$= -\int_B^0 ((\partial p/\partial y)/\rho)dz + \tau_w{}^y/\rho - \tau_B{}^y/\rho \quad (1)$$

$$0 = \int_B^0 (\partial\phi/\partial y)dz - \tau_w{}^y + C_D|\mathbf{v}|\mathbf{v} \quad (2)$$

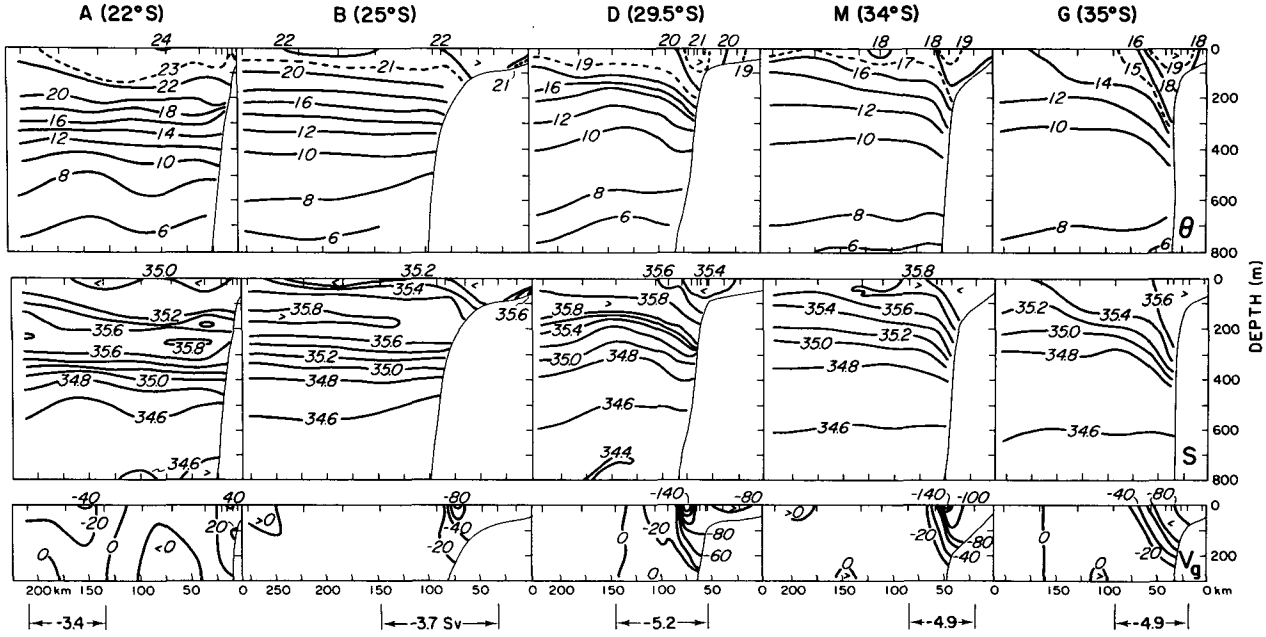

FIG. 16. Vertical sections of potential temperature, salinity, and geostrophic velocity (relative to 300 db) at five latitudes during 4–19 Aug 1987. The extrapolation technique described by Reid and Mantyla (1976) was used to calculate velocities in shallow water. The alongshore geostrophic transport between indicated limits is shown at the bottom.

TABLE 5. The onshore and alongshore volume transports (Sv ≡ 10^6 m^3 s^{-1}) obtained by vertically integrating the geostrophic velocity relative to 300 db. The onshore transports are across the lines joining the most offshore stations of the principal CTD sections, (the length of each line in km is given); entries in italics give the corresponding wind-driven surface Ekman transport. The alongshore transports (negative poleward) are between the 80 m isobath and the most offshore station of each section (with their separation in km); entries in italics are estimates of the Leeuwin Current transport (and the separation between stations spanning it).

Onshore transports

	A to B (22°–25°S)	B to D (25°–30°S)	D to M (30°–34°S)	M to G (34°–37°S)
Sep 1986	2.0 (340)	4.5 (670)	−0.1 (440)	−0.2 (330)
	−0.3	*−0.2*	*−0.1*	*0.1*
Jan–Feb 1987	—	2.2 (680)	1.0 (430)	−0.2 (370)
		−0.6	*−0.4*	*−0.3*
Mar 1987	2.2 (340)	2.3 (680)	0.5* (250)	—
	−0.2	*−0.2*	*−0.1*	
Jun 1987	—	—	1.0 (430)	1.2 (300)
			0.1	*0.2*
Aug 1987	4.4 (330)	2.2 (690)	1.2 (430)	−0.1 (370)
	−0.03	*0.03*	*0.01*	*0.04*

Alongshore transports

	A (22°S)	B (25°S)	D (29.5°S)	M (34°S)	G (35°S)
Sep 1986	1.6 (203)	−2.7 (255)	−4.8 (157)	−0.6 (193)	0.0 (33)
		−4.2 (115)	*−4.1 (50)*	*−1.6 (36)*	
Jan–Feb 1987	—	−2.4 (255)	−1.3 (160)	−1.2 (184)	−0.4 (179)
		−1.8 (59)	*−1.4 (50)*	*−1.3 (28)*	*−0.8 (31)*
Mar 1987	−4.0 (203)	−3.1 (254)	−5.9 (178)	−4.4* (186)	—
	−4.1 (92)	*−4.2 (131)*	*−6.2 (102)*	*−4.6* (84)*	
Jun 1987	—		−6.5 (158)	−4.2 (152)	−4.2 (71)
			−6.8 (88)	*−5.1 (114)*	*−4.2 (71)*
Aug 1987	−1.4 (330)	−4.9 (264)	−4.7 (161)	−5.0 (194)	−5.0 (180)
		−3.7 (115)	*−5.2 (89)*	*−4.4 (63)*	*−4.9 (73)*

* Because there was no M section on this cruise, we used a section near Fremantle (32°S) instead.

where ϕ is the geopotential anomaly (dynamic height), B is the bottom depth, $\tau_w{}^y$ is the wind stress, and $\tau_B{}^y$ is the bottom stress, C_D is a dimensionless drag coefficient, and $\mathbf{v}$ is the velocity above the bottom boundary layer.

The first term on the right-hand side of Eq. (2) is the vertical integral of the alongshore gradient of geopotential anomaly and represents the onshore geostrophic transport in the layer extending from the surface to the bottom. To estimate this term, we rewrite it as the alongshore gradient of the vertically integrated geopotential anomaly between the surface and some depth Z, i.e.,

$$\int_Z^0 (\partial\phi/\partial y)dz = \partial(\int_Z^0 \phi dz)/\partial y = \partial P/\partial y, \quad (3)$$

where $P(Z) = \int_Z^0 \phi\, dz$ can be evaluated at each CTD station for various values of Z. Its alongshore gradient, $\partial P/\partial y$, can be estimated by regression of P on latitude. Figure 18a shows the value of $\partial P(Z)/\partial y$ as a function of the layer depth Z, calculated from stations just offshore of the 2000 m isobath using a reference level of 1300 db: its maximum value lies between 200 and 250 m, and its value at 1300 m is essentially zero ($0.4 \pm 1.2 \times 10^{-4}$ m s^{-2}). At depths shallower than the maximum $\partial P(Z)/\partial y$, the geostrophic flow is onshore, and at deeper depths the geostrophic flow is offshore (see also Fig. 17). Near the 2000 m isobath, the onshore transport is approximately balanced by the offshore transport. Near the coast, where the bottom depth is less than 250 m, the onshore geostrophic transport must be balanced entirely by offshore Ekman transport in the surface and bottom layers if the flow regime is uniform along the coast. The maximum v would occur over the isobath corresponding to the depth for which $\partial P/\partial y$ is a maximum (Thompson 1987).

To evaluate the terms in Eq. (2) near the core of the Leeuwin Current (Table 6), we used the CTD stations along the 500 m isobath to estimate $\partial P/\partial y$ by integrating the geopotential anomaly relative to 300 db from the sea surface to 200 m; the alongshore profile of P is shown in Fig. 18b. The wind stress was estimated by averaging the wind stress time-series of all stations between Carnarvon and Cape Naturaliste for 36-day periods encompassing each CTD cruise. The bottom stress given in Table 6 is that required to balance the other two terms of Eq. (2), and the inferred current, v_i, is estimated by assuming a square-law for bottom stress ($\tau_B{}^y = C_D|\mathbf{v}|\mathbf{v}$) and a dimensionless drag coef-

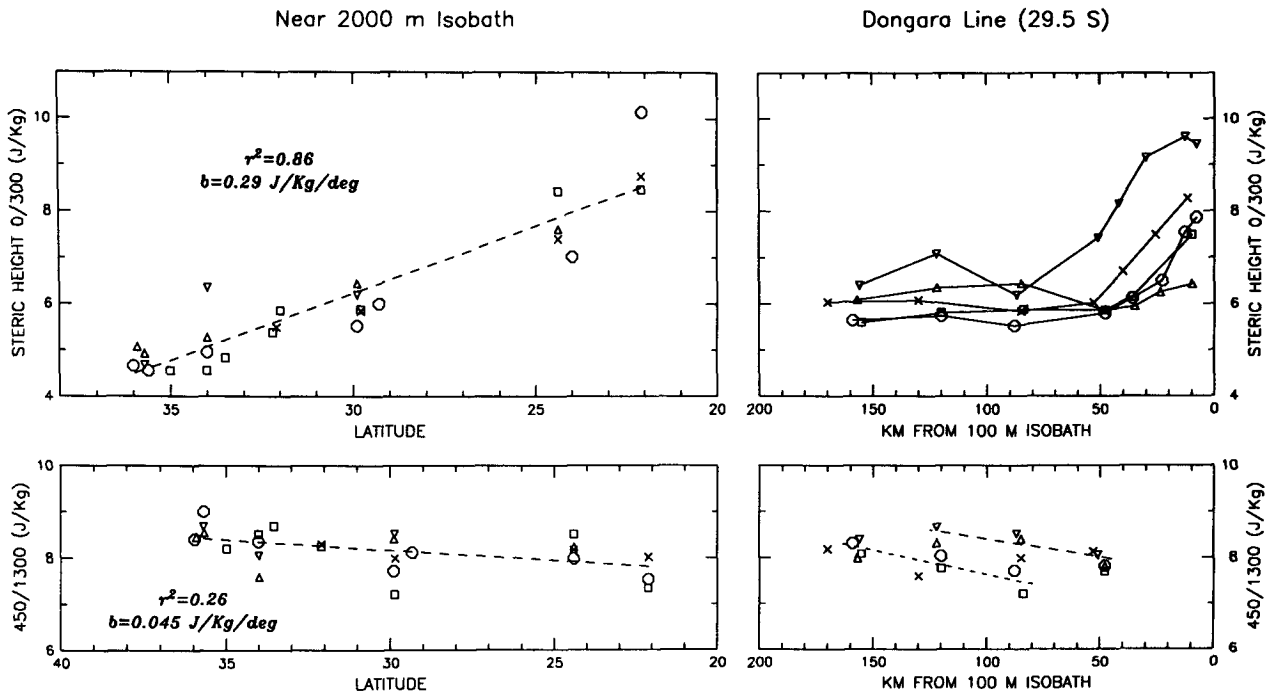

FIG. 17. Alongshore and zonal profiles of the geopotential anomaly between the surface and 300 db, and between 450 and 1300 db, during 4–18 Sep (squares), 27 Jan–14 Feb (triangles), 12–22 Mar (x's), 3–17 Jun 1987 (inverted triangles), and 4–19 Aug 1987 (circles). The alongshore profiles, with regression lines (dashed) are for stations just offshore of the 2000 m isobath. The zonal profiles off Dongara (at 29.5°S) include only stations that sampled to at least 300 db; regression lines were calculated for the inshore stations of the February and June sections (dashed line) and for the offshore stations of the September and August sections (dotted line).

ficient of 1.5×10^{-3}. Both the inferred currents (v_i) and 36-day averages of the observed currents (v_o) over the 300 m isobath (the D3 mooring) are shown in Table 6.

Profiles of the vertical integral (0 to 200 m) of geopotential anomaly (relative to 300 db) along the 500 m isobath (Fig. 18b) show that the general alongshore trend during each cruise is about the same as the slope of the least-squares fit to all the data, i.e., $2.5 \pm 0.5 \times 10^{-4}$ m s^{-2}. During the February and March cruises, local gradients are quite uniform along the coast, but in June, August and September, some local gradients

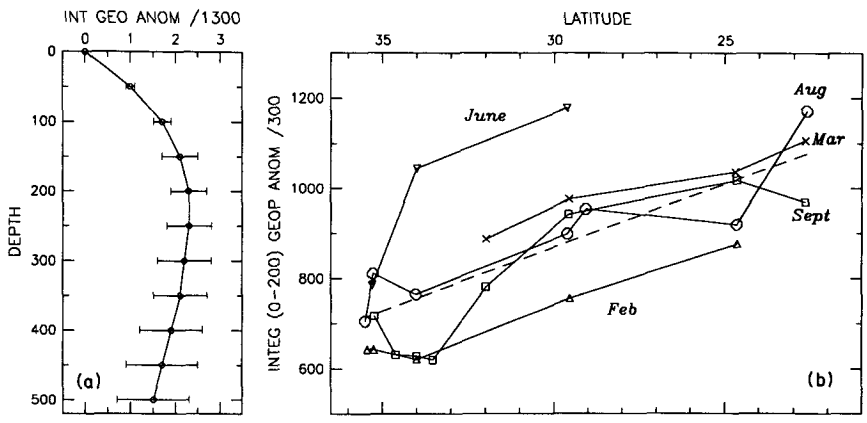

FIG. 18. (a) The value of $\partial P(Z)/\partial y$ in units of 10^{-4} m^2 s^{-2}, as a function of the integration depth, Z. Values and confidence limits at each 50 m depth increment were obtained by linear regression (on latitude) of the vertical integral of the geopotential anomaly relative to 1300 db for stations offshore of the 2000 m isobath (same stations as in Fig. 17). (b) Alongshore profiles of the vertical integral (0 to 200 m) of the geopotential anomaly relative to 300 db, for stations along the 500 m isobath, for the five hydrographic cruises. The regression line (dashed) was calculated from the combined dataset of 27 stations.

TABLE 6. Estimates of terms in the alongshore momentum balance during the five hydrographic cruises. The first column is the vertical integral (0 to 200 m) of the alongshore gradient of geopotential anomaly (relative to 300 db) between the 500-m-isobath stations on the D and M lines (29.5° and 34°S); the large-scale gradient (estimated by least-squares fit for each cruise) is shown in parentheses. The wind stress (τ^w) is the alongshore-averaged stress for a 36-day period including the CTD cruise. The bottom stress (τ^b) is the difference between the first two columns, v_i is the alongshore current inferred from this bottom stress, and v_0 is the 36-day average current at D3/129. The bottom row uses the gradient obtained by least-squares fit over all cruises, and the 325-day average values for τ^w and v_0.

	$\partial P/\partial y$	τ^w	τ^b	v_i	v_0
	($\times 10^{-4}$ m^2 s^{-2})			(m s^{-1})	
September 1986	6.4	0.2	6.2	−0.64	—
	(2.8 ± 0.6)	(0.2)	(2.6)	(−0.42)	
Jan–Feb 1987	2.7	0.7	2.0	−0.36	−0.19
	(2.0 ± 0.2)		(1.3)	(−0.29)	
March 1987	3.3*	0.3	3.0	−0.45	−0.44
	(1.9 ± 0.3)		(1.6)	(−0.33)	
June 1987	2.7	−0.1	2.8	−0.43	−0.21
	(5.3 ± 2.8)#				
August 1987	2.7	0.0	2.7	−0.42	—
	(2.4 ± 0.5)		(2.4)	(−0.40)	
Overall	2.5 ± 0.5	0.3	2.2	−0.38	−0.30

* Since there was no M line on this cruise, a station at 32°S was used instead.
\# This estimate is based on only three stations: at 29.5°, 34° and 35.2°S.

differ appreciably from the overall trend; in September the local gradient between 29.5°S and 34°S is about twice the large-scale gradient (Table 6). Such strong local gradients probably reflect meanders or eddies of the Leeuwin Current. For example, the offshore position of the Leeuwin Current core off Dongara in June (Fig. 10) is reflected in the high values of the integrated geopotential anomaly over the 500 m isobath at both 29.5° and 34°S (Fig. 18), and the rapid drop in integrated geopotential anomaly between 34° and 35°S indicates the Leeuwin Current turning inshore there; observations farther downstream (Cresswell and Peterson 1991) show the Leeuwin Current near the shelf-break at this time. Apart from such local variations in the alongshore gradient, the LUCIE data show no significant "seasonal" variation in the first term of Eq. (2), $\partial P/\partial y$. In contrast, Godfrey and Ridgway (1985) obtained a large seasonal variation in $\partial P/\partial y$ between 22.5° and 32.5°S from historical hydrographic data; their Fig. 11 shows that $\partial P/\partial y$, using a larger vertical interval (0 to 450 m) and the geopotential anomaly relative to 1300 db, varies from -0.2×10^{-4} m s^{-2} in January to 2.6×10^{-4} m s^{-2} in May. With the same integration depth and reference level as Godfrey and Ridgway, the LUCIE data yield an overall value of $1.7\ (\pm 0.8) \times 10^{-4}$ m s^{-2} with no seasonal variation. The discrepancy is intriguing. Closer examination shows that Godfrey and Ridgeway (1985) are in agreement with the LUCIE data, and with Hamon (1965), in having no seasonal variation in the alongshore gradient of steric height at the sea surface; the seasonal contribution to their estimate of $\partial P/\partial y$ is from subsurface levels, where the alongshore gradients are smaller and sampling noise is relatively large. Godfrey and Ridgway (1985) used all available data, including XBTs, to estimate P at the center of 5° × 2.5° rectangles, whereas the estimates for LUCIE are calculated directly from CTD stations along a common isobath. There is some evidence that LUCIE took place in an anomalous year (discussed in Conclusions) and the resolution of the question whether $\partial P/\partial y$ usually varies seasonally enough to significantly affect the balance in Eq. (2) requires a few years of repeated CTD observations over the continental slope.

The LUCIE CTD sections off Dongara at 29.5°S (Fig. 10) provide evidence that the Leeuwin Current does vary seasonally, with geostrophic transports ranging from <2 Sv in February to >6 Sv in March and June (Table 5). In March, the core of the Leeuwin Current was near the shelf break (Fig. 10), and is reflected in strong currents at D3 (Fig. 4); in June, the Leeuwin Current was farther offshore, and currents at D3 were relatively weak (Fig. 4). From Table 6 we conclude that the seasonal variation of the Leeuwin Current may be caused by the alongshore wind stress, which varies from near zero in June and August to 0.7 dyn cm^{-2} in February. However, current and wind measurements must be made for more than a year to establish a causal seasonal relationship with confidence. The wind stress values in Table 6 were calculated from coastal wind data assuming neutral stability (Forbes and Morrow 1989), and may underestimate the actual wind stress over the Leeuwin Current. The coastal winds in the October to February period of relatively strong equatorward winds (Fig. 2) are low compared with historical ship observations (KNMI 1949) and the ship's log for the February cruise. As a result, we probably overestimate the bottom stress required for dynamical balance, and hence the inferred current, for February (Table 6).

The drag coefficient, C_D, used to obtain the inferred velocity from bottom stress, was assumed constant in Table 6; however the actual bottom stress near the shelf break probably depends on the amplitude of long-period (12-20 s) surface waves (Grant and Madsen 1979; Grant et al. 1984). No wave measurements were made off Western Australia during LUCIE, but wave-climate data from the west coast of Tasmania show the 12-20 s surface wave energy to be small in summer and large in winter (John Reid, personal communication); this suggests that $C_D > 1.5 \times 10^{-3}$ in June, August and September, and hence that values of v_i for these months are probably overestimates.

The 36-day averages of the currents measured at D3/129 (available only for the February, March and June cruises, since current meters were deployed or recovered on the other two cruises) are in qualitative agreement with the inferred bottom currents. Table 6 shows the inferred bottom velocity is poleward between 0.2 and 0.7 m s^{-1} in all cases, i.e., generally consistent with average velocities in the core of the Leeuwin Current (Tables 2, 3; Figs. 5, 9). Given the uncertainties in the wind stress and the appropriate drag coefficient for bottom stress, the agreement between the inferred velocities and those observed during LUCIE is as good as we might expect. We conclude that the LUCIE data are consistent with the proposed momentum balance [Eq. (1)] on seasonal and longer time scales.

One consequence of this momentum balance is the diminution or suppression of coastal upwelling under the equatorward winds. The onshore geostrophic flow near the surface is sufficient to overwhelm the offshore-directed Ekman transport: From Fig. 18 we see that the onshore geostrophic transport in the upper 50 m, viz., $f^{-1}\partial P/\partial y$, is 1.4 m^3 s^{-1} per alongshore meter; the Ekman transport, $f^{-1}\tau_w{}^y$, using the average wind stress, $\tau_w{}^y = 0.3$ dyn cm^{-2}, is -0.4 m^3 s^{-1} per alongshore meter. The CTD data during LUCIE indicate that the surface layer over the outer shelf and upper slope is nearly homogeneous to a depth of at least 30 m in summer (January/February) and to more than 100 m in winter (September, June and August). Even if the Ekman transport was concentrated in a shallower layer (20 m), the onshore geostrophic transport in this shallower layer would be enough (0.6 m^3 s^{-1} m^{-1}) to suppress any net offshore transport in the surface layer, and hence coastal upwelling, except during very high wind speeds ($\tau_w{}^y \approx 1$ dyn cm^{-2}). Thus, the alongshore pressure gradient is the cause of the lack of coastal upwelling along the western Australia coast. Suppresion of upwelling due to an alongshore pressure gradient is unusual in other eastern boundary regions, but has also been observed off Peru during El Niño (Huyer et al. 1987).

Our analysis of the momentum balance [Eq. (1), Table 6] indicates that bottom friction plays an important role in the dynamics of the Leeuwin Current. To investigate this further, we examine the vertical profile of the current at the shelf-break moorings, D2 and DM, which together provided measurements at six depths from February to August 1987. (Unfortunately, vertical coverage was poor at D3 and D4, near the core of the Leeuwin Current). Profiles are shown (Fig. 19) for two 72-day periods representing the season of moderate upwelling-favorable winds and the season of weak alongshore winds. (Data above 48 m were not available for the earlier season of strong upwelling-favorable winds). The mean alongshore current is nearly independent of depth between 8 and 92 m, though there is a suggestion that the mean positive wind stress (0.32 dyn cm^{-2} at Carnarvon) retards the surface current in the March–May period. Near the bottom, the strength of the alongshore current decreases rapidly, from about 18 cm s^{-1} at 92 m, to 8 cm s^{-1} at 102 m, and (presumably) to zero at the bottom (107 m). The mean currents have a strong offshore component near the bottom in both seasons. The profile of the alongshore current suggests the thickness of the bottom boundary layer is between 15 and 33 m in both seasons, but the depth of the layer with $u < 0$ is greater during the March–May period than during the May–July period in spite of stronger stratification during the former (Fig. 19). The offshore flow in the bottom boundary layer is stronger in the May–July period than the March–May period (although the alongshore flow is weaker), perhaps because of stronger bottom drag induced by long-period surface waves generated by winter storms over the Southern Ocean. We can estimate the drag coefficient, C_D, from the total offshore transport, M_{xB}, between the bottom and the depth at which $u = 0$, assuming $M_{xB} = f^{-1}\tau_B = f^{-1}C_D v^2$. For the March–May period, we obtain a value of $C_D = 1.5 \times 10^{-3}$ (using v_{47}, where $u = 0$) or $C_D = 2.9 \times 10^{-3}$ (using v_{92}, 15 m above the bottom); for the May–July period, $C_D = 9.0 \times 10^{-3}$ (using v_{72}, where $u = 0$), or $C_D = 5.6 \times 10^{-3}$ (using v_{92}). These values are all within the range of C_D observed in other shelf regions (Winant and Beardsley 1979). Clearly, there is considerable uncertainty in the actual bottom drag, but it is definitely greater during the May–July (winter) period, consistent with the surface wave climate.

At depths shallower than 60 m, the mean currents at D2 (Fig. 19) are weakly onshore, with speeds of a few cm s^{-1}, consistent with the positive alongshore pressure gradient (Figs. 17, 18). Near the surface, the mean onshore flow is retarded or reversed by wind-driven offshore transport in a thin Ekman layer. The "wind-driven" offshore transports above 13 m (estimated at 0.56 m^2 s^{-1} in the March–May period and 0.23 m^2 s^{-1} in the May–July period, by extrapolating the lines connecting u_{13} to u_8 and u_{47} to u_{13}) are greater than those estimated directly from the wind-stress data of Table 1 (e.g., 0.44 and 0.11 m^2 s^{-1} for the March–May and May–July periods, respectively, using the wind stress at Carnarvon); this provides further evidence that wind stress has been underestimated. In the

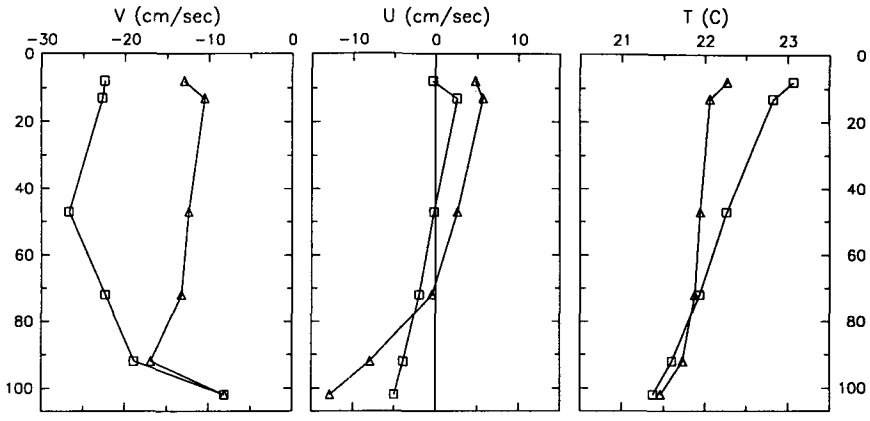

FIG. 19. Vertical profiles of the average alongshore (v) and onshore (u) components of the current and the average temperature at the 29.5°S shelf-edge moorings, DM and D2, for two 72-day periods: 1 Mar–12 May (squares), and 20 May–31 Jul (triangles). Negative currents are poleward or offshore.

March–May period, the onshore transport of 0.47 m^2 s^{-1} (calculated by assuming that u varies linearly between current meters) is less than the total offshore transport (1.65 m^2 s^{-1}); the apparent deficit would disappear if the actual mean u between 13 and 47 m were 3.5 cm s^{-1} greater than our estimate—this is a definite possibility given the absence of data in this layer. Perhaps fortuitously, during the May–July period, the total onshore transport (2.3 m^2 s^{-1}) very nearly balances the total offshore transport (2.2 m^2 s^{-1}).

The offshore transport in the bottom Ekman layer is expected to be even greater along the upper continental slope between D2 and D3, where the average alongshore velocity is 50%-100% stronger (Fig. 5). Offshore velocities of 5 to 10 cm s^{-1} in an Ekman layer along the steep bottom slope (2% between D2 and D3) will have a vertical velocity component of −0.1 to −0.3 cm s^{-1} (−80 to −250 m day^{-1}). Such downward velocities are stronger than those occurring during typical coastal downwelling events driven by poleward winds, and must be important in downwarping isopycnals and isotherms, and in maintaining the bowl-shaped contours observed in winter, e.g., off Dongara in September, June and August (Fig. 10) and along the B, D, M, and G lines in August (Fig. 12). As indicated by Thompson (1987), the strong bottom Ekman transport and downwelling are also mechanisms for maintaining and intensifying the negative onshore density gradient, and hence, through geostrophy, the vertical shear and the poleward surface current.

7. Conclusions

The nearly year-long current meter measurements made across and along the shelf edge off Western Australia between September 1986 and August 1987, and the associated CTD surveys, showed poleward flow (the Leeuwin Current) above 250 m throughout the year. A narrow equatorward undercurrent along the continental slope was apparent in the current meter data between 250 and 450 m, but not clearly resolved in the CTD sections. Although there was seasonal variation, the poleward Leeuwin Current flowed during all seasons. Throughout the year, and along the entire Western Australian coast, there is a local temperature maximum at the core of the Leeuwin Current. At latitudes north of about 32°S, the core of the Leeuwin Current forms a salinity minimum. Between 29° and 34°S, the Leeuwin Current seems to entrain high-salinity subtropical waters from offshore. Farther poleward, offshore waters are relatively fresh and the core of the Leeuwin Current appears as a salinity maximum as well as a temperature maximum. The Leeuwin Current was strongest near the shelf edge in late summer and early autumn (March–May) and farther seaward in winter (June–August). It was weaker, and near the shelf edge, in spring (September–December) and almost vanished in early summer (January). The seasonal variation seems to be due to the seasonal variation in the wind stress, which is most strongly equatorward in spring and summer, rather than to any seasonal variation in the alongshore pressure gradient. The alongshore pressure gradient was nearly the same for the five CTD surveys (there was no cruise during spring, however) and agreed with Hamon's (1965) earlier "seasonal" study.

The strong, narrow Leeuwin Current depends on the alongshore pressure gradient of the Eastern Indian Ocean, which "drives" an onshore geostrophic transport in the upper 250–300 m, between about North West Cape (22°S) and Cape Leeuwin (35°S). Offshore of the upper continental slope, and offshore of the Leeuwin Current core, the onshore transport in the upper layer is balanced by offshore transport in a deeper layer; the vertically averaged geostrophic transport

across the 2000 m isobath (relative to 1300 or 1750) is close to zero. Near the shelf break, the onshore geostrophic flow of the upper layer cannot be balanced by offshore geostrophic transport, and is greater than the offshore Ekman transport in the surface layer due to the equatorward wind stress. Instead the onshore transport is balanced (or nearly balanced) by offshore Ekman transport in the bottom boundary layer under the poleward Leeuwin Current.

LUCIE was conducted during an apparently "normal" period in terms of wind stress and alongshore gradient of the surface dynamic height. However, Alan Pearce (personal communication) has pointed out that the Southern Oscillation Index (SOI), the subsurface temperature on the continental shelf monitored near Rottnest Island (32°S), and the monthly mean sea levels at Fremantle were all lower during 1986 and 1987 than their long term mean. These have been used as indices of the strength of the Leeuwin Current by Pearce and Phillips (1988), and would indicate a weaker than average Leeuwin Current during the LUCIE experiment. Indeed, Fremantle sea level was at its lowest during December to February, which was the period when the Leeuwin Current was weakest. Since LUCIE was the first study to make quantitative estimates of the transport of the Leeuwin Current, a quantitative relation between the indices and the transport does not yet exist. Whether the Leeuwin Current during "normal" SOI times has a transport significantly greater than the 4 to 5 Sv measured during LUCIE is unknown.

Acknowledgments. The tide gage data for Fremantle were supplied by the Tidal Laboratory of the Flinders Institute for Atmospheric and Marine Sciences. We benefited from the expert computer assistance given by Neil White (CSIRO Division of Oceanography) and Rich Schramm (Oregon State University College of Oceanography, now at Monterey Bay Aquarium Research Institute), the able assistance of Jane Flesichbein (Oregon State University), and the critical readings of this manuscript by Alan Pearce, George Cresswell and two anonymous reviewers. The two authors from Oregon State University were supported by NSF Grant OCE-8709930 and the Office of Naval Research Coastal Sciences Program; this manuscript was completed while they were on sabbatical at the CSIRO Marine laboratories, enjoying the generous hospitality of the CSIRO Division of Oceanography.

REFERENCES

Andrews, J. C., 1977: Eddy structure and the West Australian Current. *Deep-Sea Res.*, **24,** 1133–1148.

Batteen, M. L., and M. J. Rutherford, 1990: Modeling studies of eddies in the Leeuwin Current: The role of thermal forcing. *J. Phys. Oceanogr.*, **20,** 1484–1520.

Boland, F. M., J. A. Church, A. M. G. Forbes, J. S. Godfrey, A. Huyer, R. L. Smith and N. J. White, 1988: Current-meter data from the Leeuwin Current Interdisciplinary Experiment. CSIRO Marine Laboratories, Report 198, 31 pp.

Church, J. A., G. R. Cresswell and J. S. Godfrey, 1989: The Leeuwin Current. *Poleward Flows along Eastern Ocean Boundaries,* S. Neshyba, C. N. K. Mooers, R. L. Smith and R. T. Barber, Eds. *Coastal and Estuarine Studies,* Springer-Verlag, **34,** 230–252.

Cresswell, G. R., and T. J. Golding, 1980: Observations of a south-flowing current in the southeastern Indian Ocean. *Deep-Sea Res.*, **27,** 449–466.

——, F. M. Boland, J. L. Peterson and G. S Wells, 1989: Continental shelf currents near the Abrolhos Islands, Western Australia. *Aust. J. Mar. Freshwater Res.*, **40,** 113–128.

——, and J. L. Peterson, 1990: The Leeuwin Current south of Western Australia. *J. Geophys. Res.*, in press.

Forbes, A. M. G., and R. A. Morrow, 1989: Meterological data from the Leeuwin Current Interdisciplinary Experiment: a data report. CSIRO Marine Laboratories Report 202, 20 pp.

Godfrey, J. S., and K. R. Ridgway, 1985: The large-scale environment of the poleward-flowing Leeuwin Current, Western Australia: longshore steric height gradients, wind stress and geostrophic flow. *J. Phys. Oceanogr.*, **15,** 481–495.

——, D. J. Vaudrey and S. D. Hahn, 1986: Observations of the shelf-edge current south of Australia, winter 1982. *J. Phys. Oceanogr.*, **16,** 668–679.

Grant, W. D., and O. S. Madsen, 1979: Combined wave and current interaction with a rough bottom. *J. Geophys. Res.*, **84,** 1797–1808.

——, A. J. Williams III and S. M. Glenn, 1984: Bottom stress estimates and their prediction on the northern California continental shelf during CODE-1: The importance of wave-current interaction. *J. Phys. Oceanogr.*, **14,** 506–527.

Griffiths, R. W., and A. F. Pearce, 1985: Satellite images of an unstable warm eddy derived from the Leeuwin Current. *Deep-Sea Res.*, **32,** 1371–1380.

Hamon, B. V., 1965: Geostrophic currents in the south-eastern Indian Ocean. *Aust. J. Mar. Freshwater Res.*, **16,** 255–271.

Holloway, P. E., and H. C. Nye. 1985: Leeuwin Current and wind distributions on the southern part of the Australian North West Shelf between January 1982 and July 1983. *Aust. J. Mar. Freshwater Res.*, **36,** 123–137.

Huyer, A., R. L. Smith and T. Paluszkiewicz, 1987: Coastal upwelling off Peru during normal and El Niño times, 1981-1984. *J. Geophys. Res.*, **92,** 14 297–14 307.

KNMI, 1949: Sea Areas Round Australia - Oceanographic and Meteorological Data. Koninklijk Nederlands Meteorologisch Instituut, Staatsdrukkerij, 'sGravenhage, 79pp.

McCreary, J. P., S. R. Shetye and P. K. Kundu, 1986: Thermohaline forcing of eastern boundary currents: with application to the circulation off the west coast of Australia. *J. Mar. Res.*, **44,** 71–92.

Pearce, A. F., and B. F. Phillips, 1988: ENSO events, the Leeuwin Current, and larval recruitment of the western rock lobster. *J. Cons. Int. Explor. Mer,* **45,** 13–21.

Reid, J. L., and A. W. Mantyla, 1976: The effect of geostrophic flow upon coastal sea elevations in the northern North Pacific Ocean. *J. Geophys. Res.*, **81,** 3100–3110.

Rochford, D. J., 1969: Seasonal variations in the Indian Ocean along 110°E, I. Hydrological structure of the upper 500 m. *Austr. J. Mar. Freshwater Res.*, **20,** 1–50.

Saville-Kent, W., 1897: *The Naturalist in Australia.* Chapman & Hall, London, 388 pp.

Thompson, R. O. R. Y., 1984: Observations of the Leeuwin Current off Western Australia, *J. Phys. Oceanogr.*, **14,** 623–628.

——, 1987: Continental-shelf-scale model of the Leeuwin Current. *J. Mar. Res.*, **45,** 813–827.

Weaver, A. J., and J. H. Middleton, 1989: On the dynamics of the Leeuwin Current. *J. Phys. Oceanogr.*, **19,** 626–648.

Winant, C. D., and R. C. Beardsley, 1979: A comparison of some shallow wind-driven currents. *J. Phys. Oceanogr.*, **9,** 218–220.

Wooster, W. S., and J. L. Reid, 1963: Eastern boundary currents. *The Sea, Vol 2.*, M. N. Hill, Ed., Wiley-Interscience, 253–280.